Design and Development of Exoskeletons for Squatting, Gait Assistance, and Fall Prevention

Applications

by

Jason S. Olson


A Dissertation Presented in Partial Fulfillment
of the Requirements for the Degree
Doctor of Philosophy


Approved March 2021 by the
Graduate Supervisory Committee:

Sangram Redkar, Chair
Thomas G. Sugar
Claire Honeycutt


ARIZONA STATE UNIVERSITY

May 2021

ABSTRACT

This research seeks to present the design and testing of exoskeletons capable of assisting with walking gait, squatting, and fall prevention activities. The dissertation introduces wearable robotics and exoskeletons and then progresses into specific applications and developments in the targeted field. Following the introduction, chapters present and discuss different wearable exoskeletons built to address known issues with workers and individuals with increased risk of fall. The presentation is concluded by an overall analysis of the resulting developments and identifying future work in the field.

DEDICATION

This work is dedicated to my wife Thien and my wonderful family, who have always been incredibly supportive and encouraging, and I could not have completed this without them.

ACKNOWLEDGMENTS

TABLE OF CONTENTS

LIST OF TABLES

LIST OF FIGURES

PREFACE

This dissertation is a composition of research that has been conducted to expand the knowledge within the field of exoskeletons and wearable robotics. Specific applications targeted and discussed within this research include gait assistance, squatting, lifting, and fall prevention. It is hoped that the design, implementation, and testing performed can be used to improve the design of exoskeleton alternatives to come.

# 1 INTRODUCTION

## 1.1. Definitions and History

The word "exoskeleton" is of Greek origin and was initially used as a biological term to describe animals with an external bone structure (MECHATECH, 2019). The word combines two parts with 'Exo' meaning outer, and 'skeleton' means the body support structure (MECHATECH, 2019). The term 'exoskeleton' has grown to encompass powered, or un-powered devices externally fitted to humans. A modern non-biological definition of an exoskeleton is a wearable device that works in tandem with the user (What is an exoskeleton?, 2019). These devices began development in the 1960s and continuously improved as technological advancements have been made (EDUEXO, 2018). General Electric is credited for developing the earliest known exoskeleton in 1965 (EDUEXO, 2018). It was designed to enable a non-disabled operator to lift heavy objects (EDUEXO, 2018). Before the 1970s, two more exoskeletons were developed to rehabilitate those with spinal injuries and provide gait assistance (EDUEXO, 2018). Since then, countless exoskeletons have been developed to assist and enhance the human body. Exoskeletons are primarily tailored to enhance a specific user or set of users in performing a particular task or series of tasks. Design goals for non-disabled users may include increasing their endurance to perform specific tasks or enabling them to perform tasks that they could not otherwise accomplish.

Many private companies share an interest in these devices for their employees to reduce workplace injuries and increase productivity. According to the Occupational Safety and Health Administration (OSHA), "Lifting heavy items is one of the leading causes of injury in the workplace (Materials Handling: Heavy Lifting, n.d.)." Workplace injuries can cost companies valuable time and productivity, damage company morale, and lead to job dissatisfaction (Barling, Kevin, & Iverson, 2003).

Exoskeletons built for those who suffer from paraplegia, paraparesis, the elderly, and those with a high risk of falling require design goals that may target restoration or augmentation of specific limbs or joints for enhanced living or rehabilitation. About fall specifically, the Centers for Disease

Control and Prevention (CDC) states that "Each year, millions of older people – those 65 and older – fall (Important Facts about Falls, 2017)." The trend of annual falls has been increasing as well, with the CDC having projected seven fall deaths every hour by the year 2030 if the present trend continues (Important Facts about Falls, 2017).

Both non-disabled and disabled individuals would benefit significantly from exoskeletons that could successfully address their need(s). The exoskeletons discussed within this dissertation focus on squatting, gait assistance, and fall prevention. The following sections discuss the background of lower-body exoskeletons and review those that target walking, squatting aid, and fall prevention, as is the goal of this research.

## 1.2. Literature Review

### 1.2.1. Walking and Gait Assistance

Walking is one of the most basic human activities and has been studied in depth at least as early as the 1940s (Vidya K. Nandikolla, 2017). One of the earliest exoskeletons developed, the kinematic walker, was built for human gait assistance (MECHATECH, 2019). The kinematic walker would eventually feature electrical motors and highlighted the importance of human locomotion in wearable robotics (MECHATECH, 2019). To develop exoskeletons, researchers first establish relationships between human muscles and body motions and have since progressed into advanced three-dimensional (3D) data collection methods and systems used today (Vidya K. Nandikolla, 2017).

Technological advancements have since allowed for creating exoskeletons, far lighter and more powerful than the earliest designs. These attributes, along with many others, are paramount for creating exoskeletons that can address real-world applications. An example of a modern exoskeleton design can be found in Wehner et al.'s publication on an exoskeleton for walking assistance (Wehner, et al., 2013). The paper presents a soft lower-extremity robotic exoskeleton aimed at healthy individuals (Wehner, et al., 2013). The design used custom McKibben style pneumatic actuators, which could assist the hip, knee, and ankle joints, and used a virtual anchor

2

for attachment points to the subject (Wehner, et al., 2013). Subject tests were performed on a treadmill and a 10-meter flat walkway (Wehner, et al., 2013). After testing, metabolic expenditures were calculated per a method described by J.M. Brockway in (Brockway, 1987) using VO2 and VCO2 data (Wehner, et al., 2013). The study results compared the user's metabolic power levels wearing the suit in its active form, in a powered-down state, in a powered state, and without the suit. The results showed almost identical metabolic costs for the active suit and the control (Wehner, et al., 2013).

A research paper by another group (Asbeck, DeRossi, Holt, & Walsh, 2015) discussed the design of a soft, biologically inspired exoskeleton that provided assistive torque to the wearer at the ankle via actuation of a Bowden cable (Asbeck, DeRossi, Holt, & Walsh, 2015). The cable had been routed from the users' back down to an attachment at the shoe (Asbeck, DeRossi, Holt, & Walsh, 2015). The exoskeleton was tested on a split-belt treadmill in a motion capture lab with walking speeds of 1.25 m/s. A pulmonary gas exchange system was used to gather O2 and CO2 gas exchange data between the subject and the environment (Asbeck, DeRossi, Holt, & Walsh, 2015). After combining the test data from all subjects under all conditions, the average metabolic reduction was 5.1% (+/-3.8%), which was statistically significant (Asbeck, DeRossi, Holt, & Walsh, 2015).

A soft exoskeleton that utilized textile materials for walking augmentation was described in (Asbeck, Schmidt, & Walsh, Soft exosuit for hip assistance, 2015). It used soft attachments instead of rigid frames or lever arms and featured retractable webbing on each leg. A backpack with motorized spools aided in hip extension via retraction of the webbing ribbons (Asbeck, Schmidt, & Walsh, Soft exosuit for hip assistance, 2015). Due to the suit's soft nature, the motors required higher speeds than that of a rigid system, which was the limiting factor of the design (Asbeck, Schmidt, & Walsh, Soft exosuit for hip assistance, 2015). The device was constructed; however, no metabolic comparison was reported.

Mooney et al. (Mooney & Herr, Biomechanical walking mechanisms underlying the metabolic reduction caused by an autonomous exoskeleton, 2016) developed an ankle-exoskeleton for walking assistance. Their goal was to discover the biomechanical mechanisms that underlie the augmentation of walking in humans, and the researchers performed walking tests on six test subjects under three test conditions. The three test conditions used were- with no assistive device, with an active assistive device on the subject's ankle, and with the same assistive device in a powered-off state. The testing results showed 11% (+/- 4%) metabolic cost reduction when compared to the cost of walking without the exoskeleton. The study also found that an ankle exoskeleton does more than reducing power at the leg but also mitigates power at the knee and hip as well (Mooney & Herr, Biomechanical walking mechanisms underlying the metabolic reduction caused by an autonomous exoskeleton, 2016).

Collins et al. have developed an unpowered exoskeleton that reduces the metabolic cost of human walking (Collins, Wiggin, & Sawicki, 2015). The exoskeleton used a tension spring, ratcheting mechanism, and clutch to offload muscle forces while walking, reducing metabolic energy consumption (Collins, Wiggin, & Sawicki, 2015). The device showed promising results of roughly a 7.2% reduction in metabolic cost while under natural walking conditions for healthy individuals (Collins, Wiggin, & Sawicki, 2015). Testing for this device was performed with each subject wearing one on each leg and walking on a treadmill at speeds of 1.25 m/s (Collins, Wiggin, & Sawicki, 2015). Electromyography data was collected on all subjects during the test and normalized with respect to their weight. Testing was performed with multiple springs stiffnesses, and results supported a hypothesis that an intermediate stiffness value would be optimal for the subjects tested, and subjects seemed to perform best at stiffness values of roughly 180 N m / rad.

1.2.2. Squatting Assistance

The second exoskeleton application to be discussed is that of squatting assistance. Although most lower-body exoskeletons primarily assist in mobility, a comparatively small number are for squatting assistance. Injuries related to lifting and squatting, particularly in a work

4

environment, can be severe, and researchers in the exoskeleton field have attempted to mitigate the risks. The paper by Yu et al. describes an exoskeleton design to prevent knee injury during squatting (Yu, et al., 2019). The paper outlines development of a powered knee exoskeleton with back-drivable quasi-direct drive actuation at the knees. An assistive profile control algorithm was created that had been derived from a biomechanics model-based control using Inertial Measurement Unit (IMU) data. The method used would then generate a biological torque profile for versatile control, including both squat and stoop lifting assistance (Yu, et al., 2019). Brushless Direct Current (BLDC) motors with high ratio harmonic gears were used to apply and assist knee torque (Yu, et al., 2019). Upon testing their device with three healthy subjects, results showed as high as an 87.5% reduction in Electromyography (EMG) for the three extensor muscles of the knee compared to that of control, which was squatting without the exoskeleton (Yu, et al., 2019).

Another exoskeleton developed for squatting and lifting assistance is that by Wehner et al. (Wehner, Rempel, & Kazerooni, Lower Extremity Exoskeleton Reduces Back Forces in Lifting, 2009). The exoskeleton used a spring mechanism and mechanical frame attached to the subject to provide a moment at the subject's hips while squatting (Wehner, Rempel, & Kazerooni, Lower Extremity Exoskeleton Reduces Back Forces in Lifting, 2009). The device was tested on six healthy subjects while lifting weighted packages. EMG testing of the device showed up to 54% less muscle activity in the subject's lower back while weighted lifting (Wehner, Rempel, & Kazerooni, Lower Extremity Exoskeleton Reduces Back Forces in Lifting, 2009).

1.2.3. Fall Prevention

Falls occur when a person is unable to maintain postural control and collides with their surroundings. Falls most commonly result in soft tissue damage and in more severe cases, fractures and death. Along with physical injuries, falls can also cause psychological trauma associated with fear of falling, leading to deficits in gait and balance, reduced physical activities, and deconditioning (Weerdesteyn, de Niet, van Duijnhoven, & Geurts, 2008). Various fall prevention methods have been investigated, including early fall detection, prehabilitative therapy,

lower-body exoskeletons designed for trajectory correction, and more (Miller, Najafi, & Armstrong, 2015), (Deng, et al., 2019). A paper by Wang et al. details the investigation into using a mechanical exoskeleton, fall detection system, and airbag deployment for fall injury reduction (Wang, Jiaxing, & Shuwen, 2021). Although the system's development has not yet been finished, the algorithm could distinguish between fall and typical human motion (Wang, Jiaxing, & Shuwen, 2021). The use of a human body posturizer (HBP) exoskeleton was also investigated for use in fall prevention (Verrusio, et al., 2017). Testing of 150 subjects showed improved short physical performance battery values and significant fall risk reduction (Verrusio, et al., 2017). Rather than broadly addressing fall prevention in general, this research has focused on specific groups of people who are more susceptible to experience fall than others, being the elderly and stroke survivors.

Although the risk of stroke increases with age, a stroke can occur at any age, and the most common type of stroke inhibits blood flow to the brain (Centers for Disease Control and Prevention, n.d.). The brain is responsible for sending motor signals to muscles through the nervous system required for muscle movement. After a stroke, these signals get affected and can delay muscle, both kinetic and kinematic responses to perturbation (Weerdesteyn, de Niet, van Duijnhoven, & Geurts, 2008). Partial or complete loss of muscle activity (paresis) in the lower limb or limbs can result in some cases. The loss of muscle activity leads to motor issues such as Drop foot (i.e., inability to lift the impaired foot during the swing phase of gait) or Spasticity (i.e., stiffness and tightening of muscles) of lower limb muscles. These issues may lead to the loss of postural control (Geurts, de Haart, van Nes, & Duysens, 2005), increasing fall risk among those affected. According to the Centers for Disease Control and Prevention (CDC), stroke is not uncommon either, with around 795,000 people in the United States suffering from stroke annually. Falls are the common complaints that individuals with such impairment have during or after their rehabilitation phase. Statistics on after-stroke falls (Batchelor, Mackintosh, Said, & Hill, 2012) reveal that 14%-65% of patients fall during hospitalization, and between 37%-73% fall during the first six months of discharge from the hospital.

The most commonly prescribed clinical remedy provided to tackle drop foot issue and improper gait is the passive thermoplastic Ankle Foot Orthosis (AFO), that is designed to lock the paretic ankle joint at a certain angle, facilitate foot clearance during swing phase, ankle stability during stance phase and heel strike. While there are reported improvements in gait velocity, stride length, and cadence(steps/min) shown after using such AFOs, studies (Nevisipour, 2019) show that continual constraints in the ankle joint adversely affect the compensatory stepping response, forward propulsion, and proprioceptive sensory information. The primary contributor to the kinetic energy and the stepping leg's speed is the forward propulsion force generated by the plantar flexor muscles. Locking the ankle joint using rigid AFOs lead to impeded forward propulsion due to restricted plantar flexion, and that can cause inhibited compensatory stepping response, inadequate foot clearance, and improper gait.

Researchers have sought to build a device to better help those with lower body impairments through research and development of AFOs capable of assisting in either muscle augmentation or rehabilitation. One such study by Yamamoto et al. detailed a semi-active AFO device aimed at hemiplegic patients, which used specialized joints with stiffness control elements, flexion stops, and a one-way friction clutch to control ankle movement in the sagittal plane (Yamamoto, Ebina, Miyazaki, Kawai, & Kubota, 1997). The AFO was tested on 33 subjects, and information was discovered concerning what AFO characteristics were most needed with hemiplegic patients (Yamamoto, Ebina, Miyazaki, Kawai, & Kubota, 1997).

A pneumatic power-harvesting ankle-foot orthosis was described by Chin et al., which attempts to combat foot-drop issues in subjects with lower-body motor-control disruptions (Chin, et al., 2009). The design incorporated a bellow pump below the foot, and a cam-lock mechanism to control relative ankle motion (Chin, et al., 2009). The testing performed on an able-bodied subject indicated that the locking mechanism used needs further refinement as excess dorsiflexion of the ankle was observed (Chin, et al., 2009). In Palmer, an active AFO used a linear torsional spring for controlling plantar flexion (Palmer, 2002). The spring would acquire elastic energy during the stance

phase loading and would release this energy during the pre-swing (push-off) phase to generate forward propulsion in the user (Palmer, 2002). The device was tested on ten healthy subjects and demonstrated that passive spring force actuation is insufficient in providing comparable power to a biological ankle (Palmer, 2002). The active AFO (AAFO) by Hwang et al. showed the use of a Series Elastic Actuator (SEA) to control ankle actuation for toe drag and foot drop prevention (Hwang, Kim, Sohn, Lee, & Kim, 2006). The SEA used an elastic element in series with a motor to generate a controlled ankle movement (Hwang, Kim, Sohn, Lee, & Kim, 2006). The device was tested on five healthy subjects and successfully prevented the toe drag of test subjects during the swing phase (Hwang, Kim, Sohn, Lee, & Kim, 2006).

Similarly, Boehler et al. described an AAFO designed for rehabilitation applications, which also used a SEA as a means of actuation (Boehler, Hollander, Sugar, & Shin, 2008). The device also allowed the user to wear their existing shoes, although due to its fastening method limiting ankle motion to the sagittal plane, the device was limiting with regard to user comfort and maneuverability (Boehler, Hollander, Sugar, & Shin, 2008). Testing was performed on a single subject, and results indicated promising open-loop control results for the novel algorithm used (Boehler, Hollander, Sugar, & Shin, 2008). Polinkovsky et al. described another AFO that uses SEA actuation to restore legged motion in patients suffering from a spinal cord injury (Polinkovsky, Bachmann, Kern, & Quinn, 2012). The AAFO reduced toe drag and foot slap of the spinal cord injury subjects tested but was mechanically unable to apply maximum torque or maximum throw in able-bodied subjects in anything faster than a slow walk (Polinkovsky, Bachmann, Kern, & Quinn, 2012). Ferris et al. presented a powered AFO that used McKibben-style pneumatic muscles for actuation and was built as a gait studying tool for post neurological injury rehabilitation (Ferris, Czerniecki, & Hannaford, An Ankle-Foot Orthosis Powered by Artificial Pneumatic Muscles). The device was shown to produce both plantarflexion and dorsiflexion of the ankle joint (Ferris, Czerniecki, & Hannaford, An Ankle-Foot Orthosis Powered by Artificial Pneumatic Muscles). It was designed to be externally supplied with electrical power and compressed air, and testing results

8

indicated that its use in physical therapy clinics might reduce the level of manual labor required by physical therapists (Ferris, Czerniecki, & Hannaford, An Ankle-Foot Orthosis Powered by Artificial Pneumatic Muscles).

1.3. Background Conclusion

Concerning walking, the challenge in creating a device capable of assisting non-disabled individuals has always been the fact that humans are so well adapted to walking. Providing walking aid typically requires adding weight to the user, which then requires higher levels of assistance to compensate. Many assistive devices reviewed did little more than compensate for their own added weight, and some, if operated with poor actuation timing or other non-ideal conditions, performed worse while worn than if they had been removed (Asbeck, Dyer, Larusson, & Walsh, 2013). Similar can be said for squatting aide and fall prevention. Although improvements in design and implementation have been made, there is still unrealized progress in the highlighted fields.

1.4. Research Goals

The broad goal of this research has been to expand the level of knowledge in the field of wearable exoskeletons. However, the primary objective has been to develop practical exoskeletons to aid users in squatting and walking activities and in fall prevention. The desire to progress in this field and change lives for the better has motivated this contribution. The testing validation methods used were based upon best practices within the field. The results and conclusions gathered are likely similar to what is to be expected from similar designs. Hopefully, this work highlights the successes and failures of these designs, such that they may influence future research that seeks the same or similar goals.

2 DESIGN OF A PASSIVE EXOSKELETON FOR SQUATTING ASSISTANCE

2.1. Background

Humans are excellent at performing physical activities such as walking and squatting; however, combining them with transporting heavy loads can result in adverse health effects,

including lower back pain (LBP). The handling of weighted materials has been associated with mechanical stresses, which can lead to LBP (Cole & Grimshaw, 2002). 60% of LBP sufferers have claimed overexertion as the cause of their injury, and certain professions, such as those who drive loaded vehicles professionally, experience up to four times the instances of LBP as that of an average person (Pope, 1989). LBP is one of the most common afflictions in today's workforce, with many afflicted workers suffering from recurring bouts (Waddell & Burton, 2001). Studies show that LBP affects blue and white-collar workers roughly equally (55.% and 51.6%, respectively) (Yildirim, Gunay, & Karadibak, 2014). While some of this can be explained through poor ergonomics in an increasingly office-centered work environment, plenty of research suggests that jobs requiring frequent lifting activities contribute to this condition. While many companies that employ this type of labor are increasingly using near-100% automation, there is still a significant human element that must be accounted for. A company that uses near-100% automation sees human injury at a rate more than double that of the national average for warehouse injuries (Evans, 2019). As more companies look to decrease costs by moving towards automation, it is clear that humans need augmentation of some kind to help reduce injuries.

To that end, design firms tend to look towards preventing LBP and related injuries. Their designs are available as active or passive solutions and claim to help reduce the risk of injury. However, many of these implementations are expensive, bulky, or too inconvenient to be utilized (Ineichen, 2019). Some of the most wide-spread designs currently focus on passive actuation, requiring no sensors or systems to activate. A worker must only don the device as recommended and continue. The leading passive devices that prevent LBP are the Laevo suit and the Personal Lift and Assistive Device (PLAD).

The PLAD was one of the first designs to be thoroughly researched; an early schematic of it can be seen in **Error! Reference source not found.** (Abdoli-E, Agnew, & Stevenson, An on-body personal lift augmentation device (PLAD) reduces EMG amplitude of erector spinae during lifting tasks, 2005). It was designed with six elastic components anchored at the shoulders and

knees. It used a novel mechanism to increase mechanical advantage by using a moment arm in the pelvis's vicinity (Abdoli-E & Stevenson, The effect of on-body lift assistive device on the lumbar 3D dynamic moments and EMG during asymmetric freestyle lifting, 2007). The testing showed that the muscular effort, as measured by EMGs, was reduced in the monitored location, but the oxygen consumption rate remained unchanged. The result implies that while a suit of this design could likely reduce a few muscles' metabolic costs, it does not reduce the whole system's metabolic cost. The researchers also suggested that the oxygen consumption was likely explained by other muscles compensating for the not assisted muscles. Then, it was possible that the extended use of this design would transfer issues causing LBP to another muscle group, causing no net gain. Further, there were issues found with the wear of the design, with users complaining of chaffing at the knees and discomfort at the shoulder.
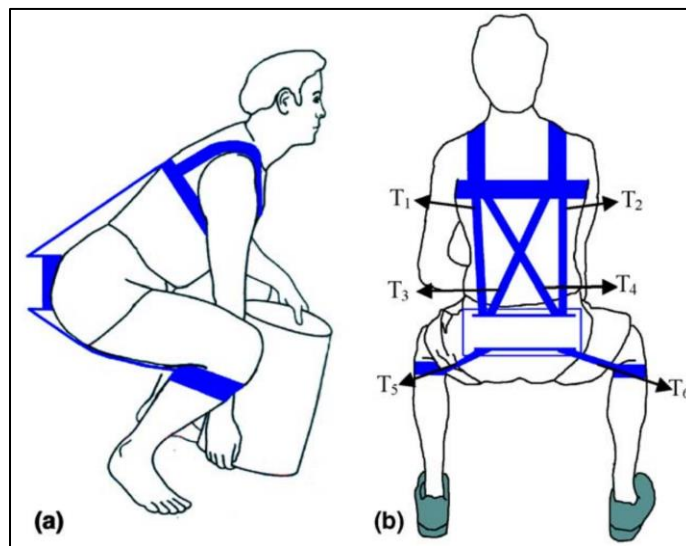


Figure 1 Illustration of The PLAD System on Squatting Subject.

Baltrusch et al. investigated the Laevo system of passive actuation, attempting to determine if the cause for the issue was PLAD-specific or indicative of passive exoskeletons as a whole (Baltrusch, van Dieen, van Bennekom, & Houdijk, 2018). This commercially available system removes the shoulder-strap anchoring used in the PLAD and places the counter pressure on a

chest plate. The knee anchors were also replaced in favor of a pad that rests on top of the thigh. A central belt connects the system through semi-rigid components that work to brace and transfer motion. After testing across multiple participants, researchers found that the exoskeleton did decrease metabolic costs by 17% when lifting from an ankle height and using a Laevo exoskeleton designed for that range of motion (Baltrusch, et al., 2019). This includes decreases in oxygen consumption, as well as associated muscle effort as measured by EMG. There were, however, complaints of fit with this device as well, with a considerable complication in the chest plate. As it grew uncomfortable, participants would reposition it, causing downstream misalignment effects (Baltrusch, van Dieen, van Bennekom, & Houdijk, 2018). This could also explain discomfort later described by users.
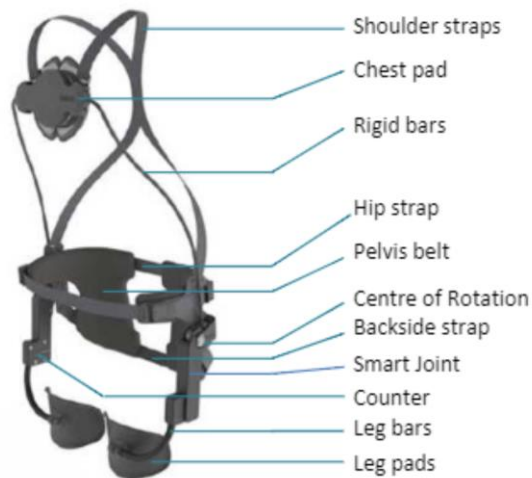


Figure 2 Laveo Exosuit Diagram. (Baltrusch, van Dieen, van Bennekom, & Houdijk, 2018)

The two types of passive exoskeletons studied showed encouraging results with consistent muscle effort decreases, particularly concerning the lower back area. However, it was clear that improvements could be made to increase comfort and address the primary problem of LBP without shifting the effort to other parts of the body.

This chapter reviews an exoskeleton's design and testing that leverages natural human motion to store and release energy via a passive means. The exoskeleton described in this chapter

is known as the Passive Load Carrying Pulley Suit (P-LCPS). The name P-LCPS stems from the single pulley featured on the back of the device and the passive nature of its operation. A novel pulley and bungee system had been devised, wherein the pulley allows the mechanism to remain virtually transparent to the user through the walk cycle. However, when the wearer performed a squatting motion, the bungees store energy during the downward movement through elongation and release to assist the upward motion through compression.

2.2. Design

The design of the P-LCPS needed to consider multiple factors, including ergonomics, motion, donning and doffing, and availability of commercial parts. Consulting with other researchers and workers helped narrow down the primary considerations to three factors. The first was comfort prioritization. If the device helped muscle function but caused discomfort in the user, it would likely never be adopted. This discomfort can be caused by pinch points, chaffing, lack of flexibility, and interaction with the device (i.e., being placed in a compromised position to don/doff).

The second focus was future device modification. While the simulations would provide initial guides and details, it was likely that configurations would need to change based on real-world data. The device prototype was built with ample room to add, remove, or rearrange components as required. This included the mechanism used to secure the elastic attachment's ends to the user, be it at the ankle or the feet.

Initial drafted designs were weighed in a decision cycle, where the above parameters were weighted most heavily. After this process, an initial prototype form was selected. The selected design would passively operate to store energy while lowering into a squat and would release it upon lifting. The support resistance would be balanced between both legs, which would be accomplished by using a single elastic element routed over a pulley and attached to each leg. The design would use a hard-backed brace complete with a waist-belt and shoulder straps for securing the device. This attachment method has been proven as an effective means of securing a load to an individual with minimal performance hindrance. The waist belt would act as the primary

anchoring point, and the shoulder straps as stabilization. This would help ensure the spine wasn't compressed needlessly. The hard-backed design would offer a generous space for attaching components and comfortable load distribution on the user.
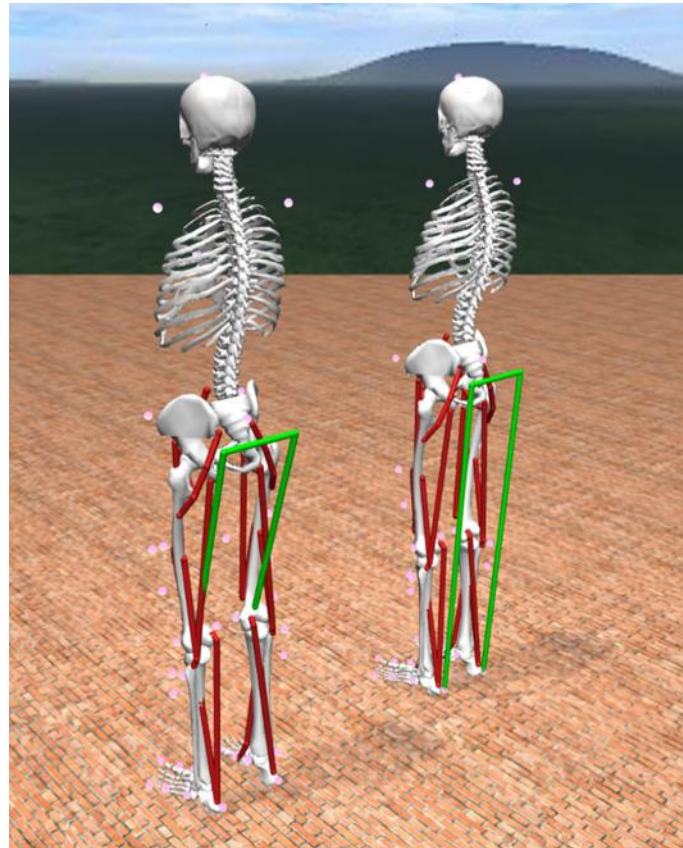


Figure 3 OpenSim P-LCPS Model

Two attachment points were simulated and analyzed using OpenSim software, as shown in Figure 3. Both arrangements were tested in OpenSim before real-world adoption. The white segments in Figure 3 represent the subject's bones, the red segments representing the essential muscles, and the green segments representing the elastic spring or bungee. The first configuration placed the attachment site about the knees of the user. The second set the attachment at the rear of the user's shoes for comparison. Parameters of the simulation were chosen to replicate best what would be achievable using available materials in the real world, including the stiffness of the bungee or path spring as modeled in OpenSim. A frictionless pulley was assumed in the model, as

only two attachment points for the bungee are required. The routing was done to account for the bungee's orientation about the user's knee.

Simulations were performed for each configuration of the P-LCPS and both under the same walking conditions. The total metabolic energy results from the simulation can be seen in the graphs below. The metabolic comparison can be seen in Figure 4.
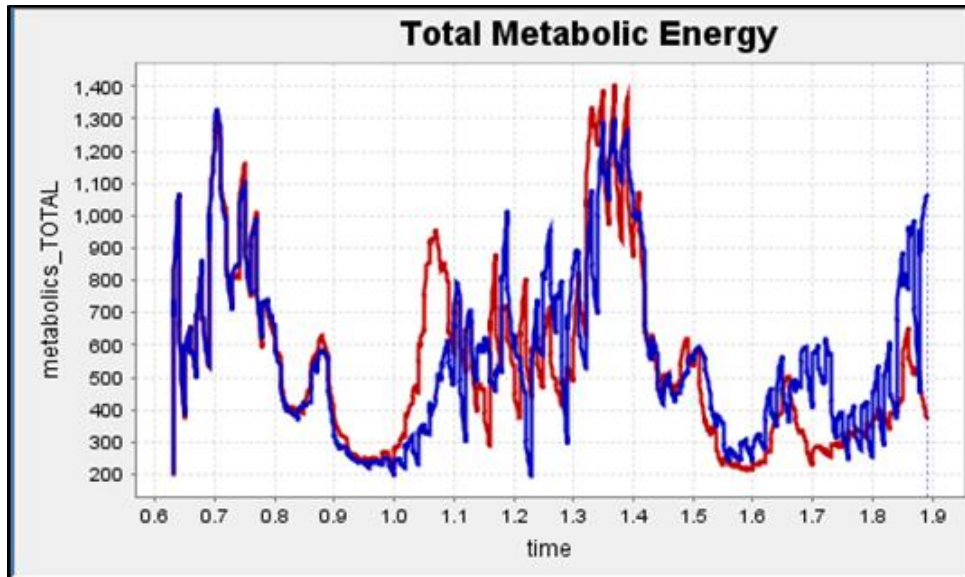


Figure 4 Opensim Simulation Results Comparing P-LCPS Knee vs. Foot Attachment .

Figure 4 shows the results of the exoskeleton with attachment points at the knees. The blue colored line represents the metabolic energy used for control with no exoskeleton, and the red colored line represents the results of wearing the exoskeleton. The plot seemingly indicated a negative impact on walking, with slight reductions in metabolic costs at some points being outweighed by increases at other points, although the trend of each is similar. Figure 5 shows the exoskeleton configuration results with attachment points at the ankles. This configuration showed very erratic differences compared to the control with relatively significant gains and losses in metabolic costs at different points in time. The results in Figure 5 indicate that the ankle attachment configuration would significantly alter the user's gait.
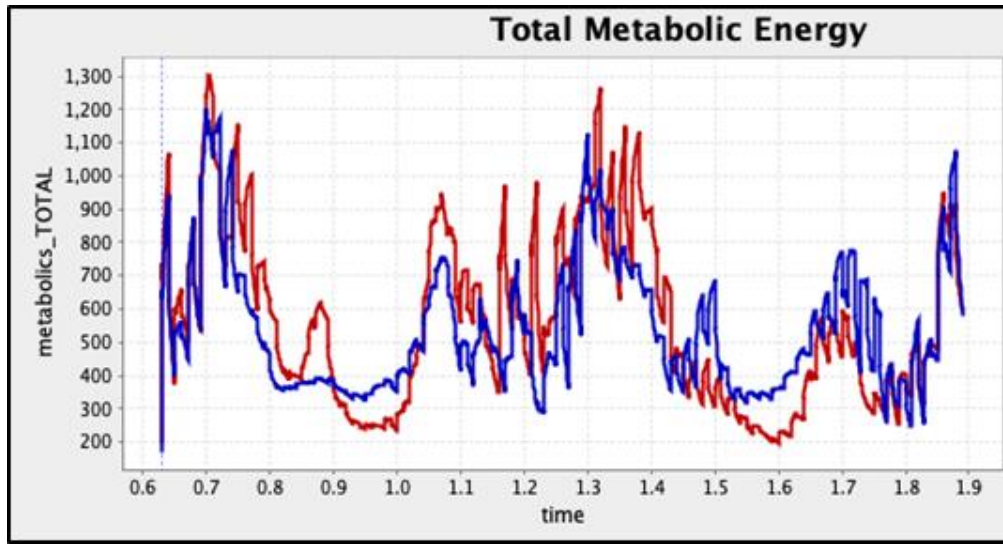
Figure 5 P-LCPS/A-LCPS Metabolic Comparison-II

Ideally, simulations for squatting would have been performed, but squatting control data would have been required as an input into the system to perform computed muscle analysis with squatting activity. This was not done as a new marker setup would have been needed and would have significantly delayed further progress. Instead of further pursuing simulations, a prototype of the P-LCPS was constructed, and testing was performed.

For construction, the P-LCPS made use of modified commercial knee brace supports with added nylon straps fixed to their back as a means of attaching the bungee. Knee braces were selected as they provided support above and below the kneecap, preventing them from loosening or chafing and offered adjustability for different users. The bungee was selected instead of a spring or other elastic means as they are relatively lightweight, durable, and easily adjustable. The stiffness of the bungee was based on commercially available materials. A buckle was added for ease of attachment and detachment when donning and doffing the suit. A pulley was made from a modified longboard wheel to retain the bungee in the desired position and featured internal ball bearings for minimal rotational resistance. The aforementioned knee attachments are shown in Figure 6, and the pulley is shown in Figure 7.

Figure 6 AAFO Knee Attachments Made from Modified Mueller Max Knee Strap.

Figure 7 Pulley Made from a Modified Longboard Wheel.

Just above the nylon straps of the knee attachments, a bungee cross strap support was added to prevent the bungees from separating and riding up the side of the users' legs while squatting. The cross-strap support fit loosely around both bungees and was positioned underneath the user while crouching. The bungee cross strap support is shown in Figure 8.

Figure 8 Bungee Cross Strap Support, Preventing Separation of te Bungees below the Bungee Guide and above the Knee Attachment.

For the remaining hardware, the P-LCPS used a lightweight U.S. military backpack frame to offer rigid support for attaching the pulley and bungee guide mechanism on the back of the subject. An aluminum plate was fixed to the support bracket to provide additional support for the pulley. The full P-LCPS assembly is shown in Figure 9.
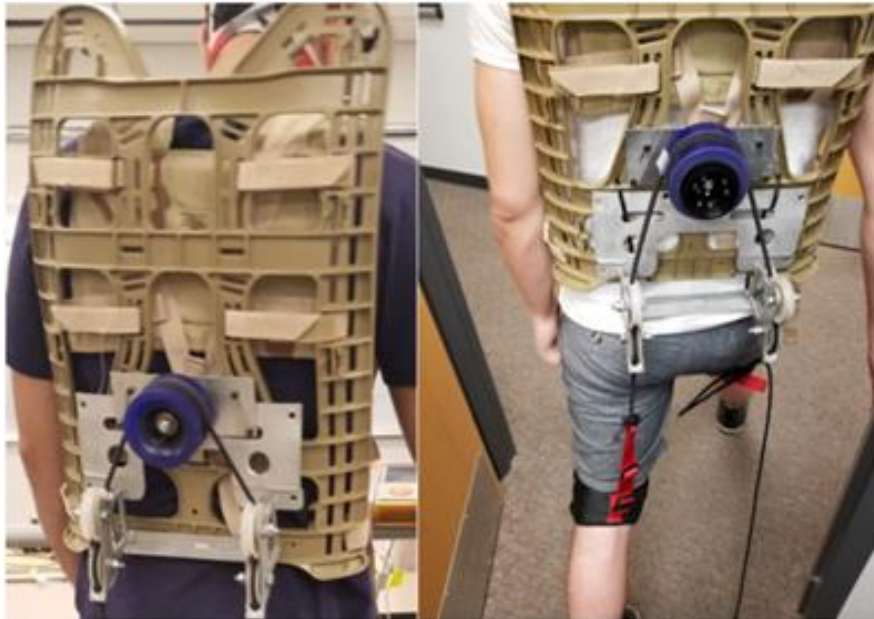
Figure 9  P-LCPS Initial Prototype Design.
The Left Image Shows the Pulley Configuration of the P-LCPS with the Pulley Guide. The Right Image Shows the P-LCPS with Knee Attachment Mid-step.

A mechanism with four small nylon pulleys was initially used to guide the bungee cable below the center pulley but would later be replaced with a loop guide to reduce friction while walking. The loop guide can be seen in Figure 10.

Figure 10 P-LCPS with 3D-printed Loose-fit Bungee Guide.

A vital feature of the P-LCPS design was the central pulley. The pulley allowed the bungee to pass with minimal resistance from one side to the other while walking in a complementary fashion. Additionally, while squatting, the bungees would be forced to extend, storing energy, which would aid in lifting. The pulley would passively and automatically balance the load on both knees and prevent potential imbalance caused by inconsistent aid on the left or right leg. This innovation helped mitigate the discomfort of having a force work against them that some users describe with exoskeletons (Ineichen, 2019).

2.3. Testing

Tests were performed on 3 healthy subjects with no history of back pain to assess the ability of the P-LCPS to reduce the metabolic cost of squatting. The data was collected via a Cosmed K5 and averaged for the test's entirety (Cosmed K5, 2019). Each test began by first

determining the participant's Resting Metabolic Rate (RMR), which was required to develop a baseline. Subjects then participated in squatting tests in a randomized order of 4 unique conditions. Condition A consisted of loaded squats while wearing the P-LCPS exoskeleton, and condition B consisted of unloaded squats while wearing the P-LCPS exoskeleton. Condition C consisted of loaded squats without an exoskeleton, and condition D consisted of unloaded squats without an exoskeleton. Loaded tests required subjects to lift a weight while squatting equal to 10% of their body weight to normalize each user's weight instead of using a static weight for all subjects. Each condition consisted of a total of 20 squats followed by a one-minute resting period. Squats were performed in rhythm to a 60 beat per minute (BPM) metronome. After 20 squats were performed, followed by the one-minute resting period, the data capture would end, and subjects would rest for an additional five minutes before the next test would be conducted.

2.4. Results And Discussion

Figure 11 shows the results of the unloaded P-LCPS tests and Figure 12 shows the results of the loaded P-LCPS tests. The P-LCPS consistently demonstrated a reduction in metabolic cost during for both loaded and unloaded tests, although the level of reduction was more substantial for that of the unloaded tests.
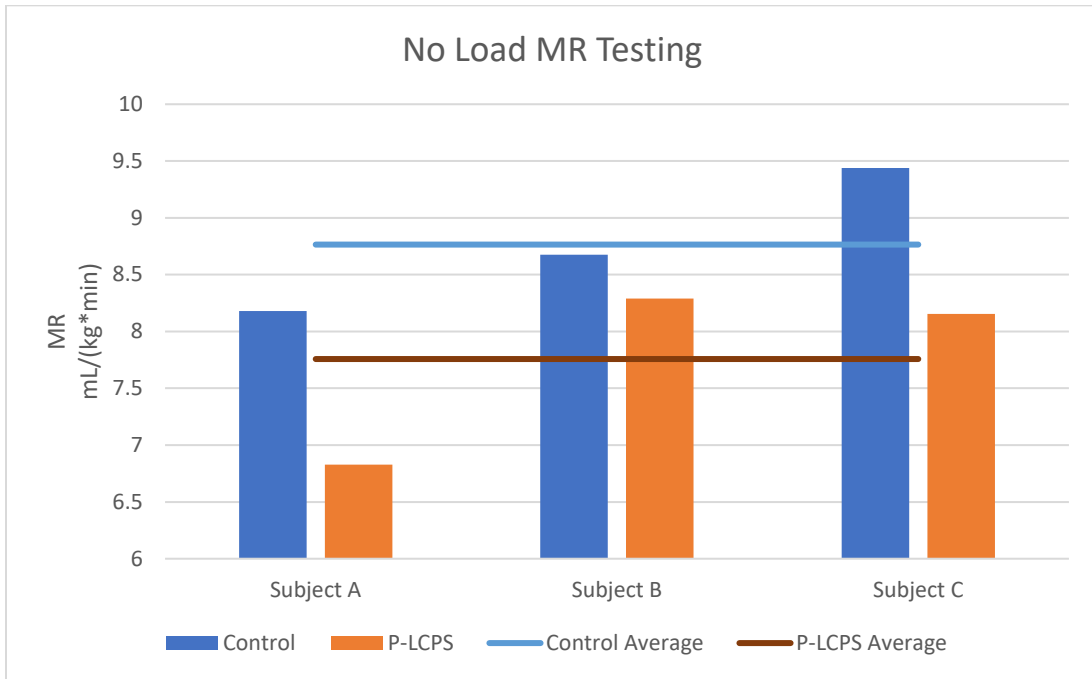
Figure 11 Metabolic Rate Results for Unloaded P-LCPS Testing
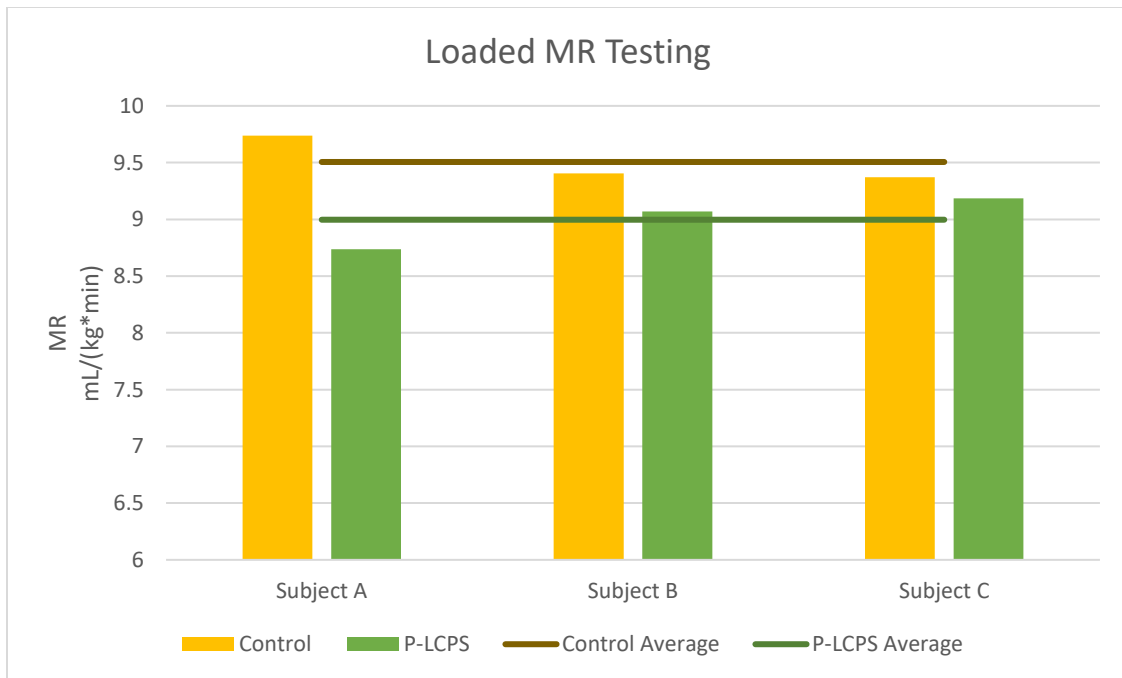


Figure 12 P-LCPS Metabolic Rate Results for Loaded P-LCPS Testing

Figure 13 shows the same data from the squatting tests shown in Figure 11 and Figure 12, organized in terms of metabolic reduction as a positive percentage. Please note that the positive percentage indicates a metabolic decrease in energy when compared to the control. The data collected suggests that there is roughly an 11.5% reduction in metabolic cost for squatting with the P-LCPS with no extra load and a 5.3% reduction in the loaded condition.
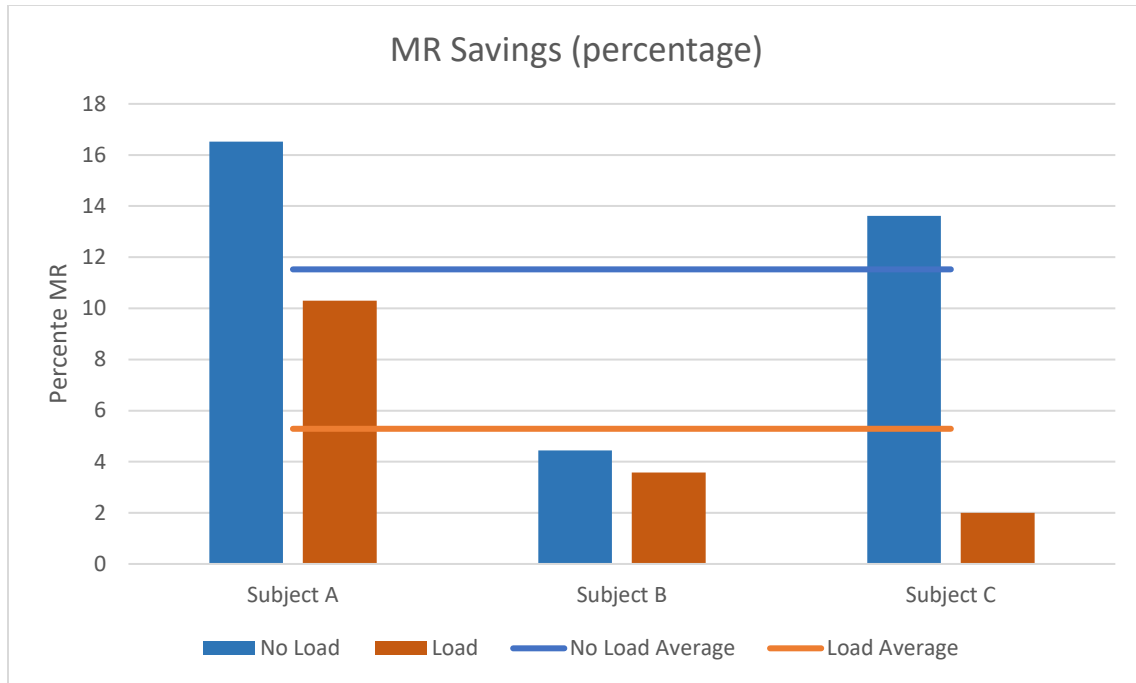


Figure 13 P-LCPS Metabolic Rate Savings

The data collected had indicated a level of promise to the design in terms of potential future applications. The testing results were in line with other research teams' efforts working with the Laevo and PLAD. There were, however, differences in the execution that led to the P-LCPS being described as comfortable, with no complaints about shoulder pain. This was encouraging as a lack of discomfort may indicate potential long-term adoption. There were also significant differences from the body of work in that this study did not focus on EMG measurements. As the null hypothesis was only interested in terms of MR, it was not necessary for this experiment.

2.5. Conclusion

This chapter examined a novel approach to LBP-relieving passive exoskeleton design. The design tested showed decreased MR when using the device over non-equipped movements of 11.5% when performing unweighted motions and 5.3% during weighted operations.

3 DESIGN OF AN ACTIVE PULLEY SUIT FOR SQUATTING ASSISTANCE

3.1. Background

This chapter builds upon the previous chapters' goals and discoveries made by developing the P-LCPS exoskeleton. For some industries and occupations, the rarity in which squats are performed, or the amount of walking or running required, may quickly diminish any exoskeleton's field application, which causes even a slight hindrance to walk performance. This chapter addresses the design and development of an active version of the P-LCPS, aptly named the Active-Load Carrying Pulley Suit (A-LCPS). The goals of the A-LCPS were to aid a non-disabled user in squatting without resisting their walking ability.

3.2. Design

The A-LCPS was based heavily on the P-LCPS, with the primary difference being the pulley's active control and secondary differences of adjustability and pulley placement as was necessary for the additional components. The A-LCPS used a motorized 3D-printed pulley with the bungee rigidly fixed to the pulley. This arrangement was necessary as the methods tried to increase friction between the pulley and motorized bungee were unreliable in maintaining sufficient bungee tension control. Fixing the bungee to the pulley offered reliable feedback on relative knee and pulley positioning, allowing the A-LCPS to avoid undesired stretching of the bungee actively. The initial version of the A-LCPS can be seen in Figure 14.
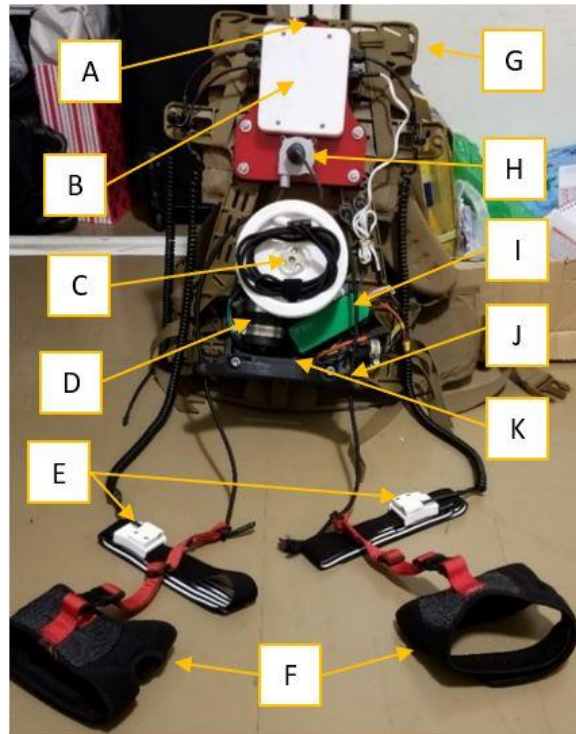
Figure 14 Labeled Diagram of A-LCPS with String-potentiometer Feedback System.
A – Power switch, B – Controller housing, C – Active pulley, D – Motor & gearbox, E – IMU(s), F
– Knee braces, G – Backpack frame, H – String potentiometer, I – LiPO Battery, J – Bungee
guide, K – Motor Controller (above bungee guide).

The basic construction of the A-LCPS was made near identically to that of the P-LCPS,

outside of the additions necessary for the pulley's motorization. As the bungee was fixed to the

pulley and therefore limited in rotation, the pulley diameter was increased from that of the P-LCPS.

This allowed for a greater range of motion of the bungee segments and reduced the motor's

required angular velocity. The A-LCPS also featured quickly adjustable bungee lengths to

accommodate users of different heights quickly and easily.

For control of the active pulley, IMUs were fixed with elastic straps to each leg above the

knee and used to measure the hip joints' angle with respect to one another in the sagittal plane.

These IMU attachments are shown in Figure 15.

Figure 15 Front View of A-LCPS.
A - IMU Attachments Were Placed on the Upper Legs, approximately Half-Way between the Hip and Knee Joints.

The value of these angles were fed to an ATmega2560 based microcontroller located on the back of the operator, above the motor. The motor used is a 12V brushed Direct Current (DC) motor with a worm drive gear reduction. A secondary pulley track was added to the back of the primary pulley, where the end of a string-potentiometer would be attached and used to provide feedback on the pulley's angular position. This feedback allowed for precise angular control of the motorized pulley. The V1 A-LCPS feedback system is seen in Figure 16.
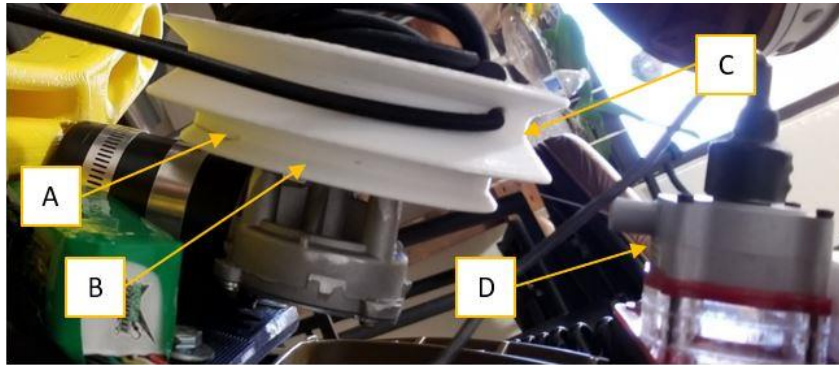
Figure 16 A-LCPS String-potentiometer Feedback System.
A – String Potentiometer String Attachment, B – Secondary Pulley, C – Primary Pulley, D – String Potentiometer. The Primary Pulley Would Guide the Bungee During Rotation, and the Secondary Pulley Would Guide the String.

This initial motor feedback setup was flawed as the string-potentiometer was vulnerable to being overextended should the motor spin in the same direction for longer than desired. Testing the system resulted in the microcontroller crashing, which led to unpredictable motor behavior and string potentiometers' overextension. A revised feedback solution was created, which involved replacing the string potentiometer with an incremental encoder coupled to the motor shaft. The advantage of this modification was that the pulley's excessive travel could no longer damage the exoskeleton. The revised A-LCPS is shown in Figure 17, Figure 18, and Figure 19.
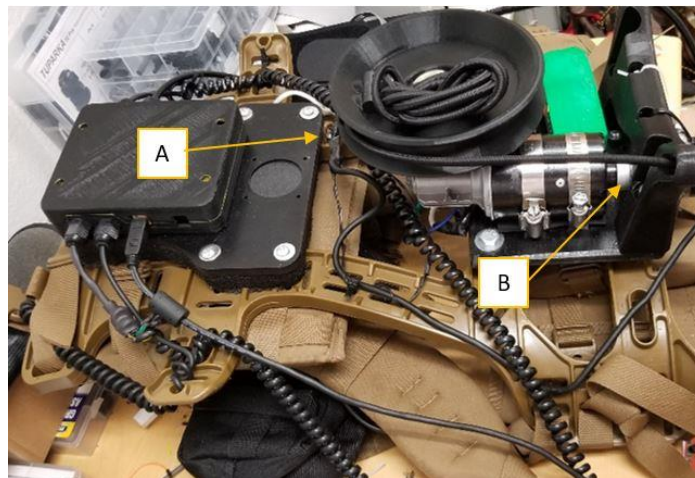


Figure 17 Complete Assembly of A-LCPS after Revisions.
A – Magnetic Switch Location, B – Incremental Encoder Location.

After the modifications were completed, angular motor control was achieved using feedback via the incremental encoder. A magnetic switch was located at the pulley's center point and tasked with notifying the controller as to when the center position of the pulley was reached. An alignment procedure would be automatically performed during the program's startup sequence and would ensure the pulley has the maximum range of motion and ensure that there would be equivalent tension on both legs while squatting. The magnet and magnetic switch components are shown in Figure 18.
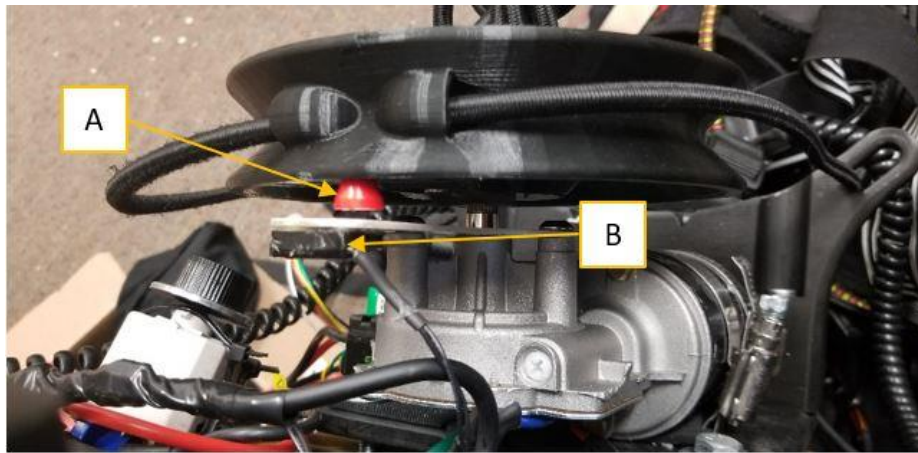


Figure 18 View of the Magnet and Magnetic Switch Located on A-LCPS.
A – Magnet, B – Magnetic Switch. Note, the Magnet Was Located at the top of the center of the Pulley. The Magnetic Switch Is Activated When Proximity to the Magnet Was Reached.

Figure 19 Post-updated A-LCPS with a View of Cross-strap and Incremental Encoder Attachment to Motor.
A – Battery Disconnect Switch, B – Bungee Cross-Strap, C – Knee Braces.

The A-LCPS exoskeleton used a Talon SRX motor controller powered by a 4000mAh 14.8V LiPO battery attached to the backpack frame. The thigh angle sensors used were two InvenSense MPU-6050 MEMS gyroscope and accelerometers. Since most thigh angle motion is in the sagittal plane, the MPU-6050 IMUs would be placed on the anterior thigh, approximately 5cm above the patella.

As a control strategy, the motor controller received input from the microcontroller, which collected data from the encoder, hip angle sensors, and magnetic switch, and used this data to follow the motion of the user with the motorized pulley, preventing unwanted resistance on the user while walking, reducing metabolic cost increases while walking and providing squatting assistance.

3.3. Testing

Testing of the A-LCPS was performed to assess the ability of A-LCPS to reduce the metabolic cost of squatting. The testing procedure performed was identical to that performed on the P-LCPS described in the previous chapter, but this time, both A-LCPS and P-LCPS

exoskeletons would be tested back-to-back for comparison. The RMR of each subject was first measured before any testing was conducted. Following that, a randomized series of 6 conditions were tested, with each subject performing a total of 20 squats in rhythm to a 60 BPM metronome (30squats/minute), then standing for one minute. The different test conditions included condition A which consisted of loaded squats while wearing the A-LCPS, and condition B consisted of loaded squats while wearing the P-LCPS. Condition C consisted of unloaded squats while wearing the A-LCPS, and condition D consisted of unloaded squats while wearing the P-LCPS. Condition E consisted of loaded squats with no exoskeleton, and condition F consisted of unloaded squats with no exoskeleton. The weighted tests used 10% of the subject's body weight to normalize the weight being lifted to the individual.

3.4. Results And Discussion
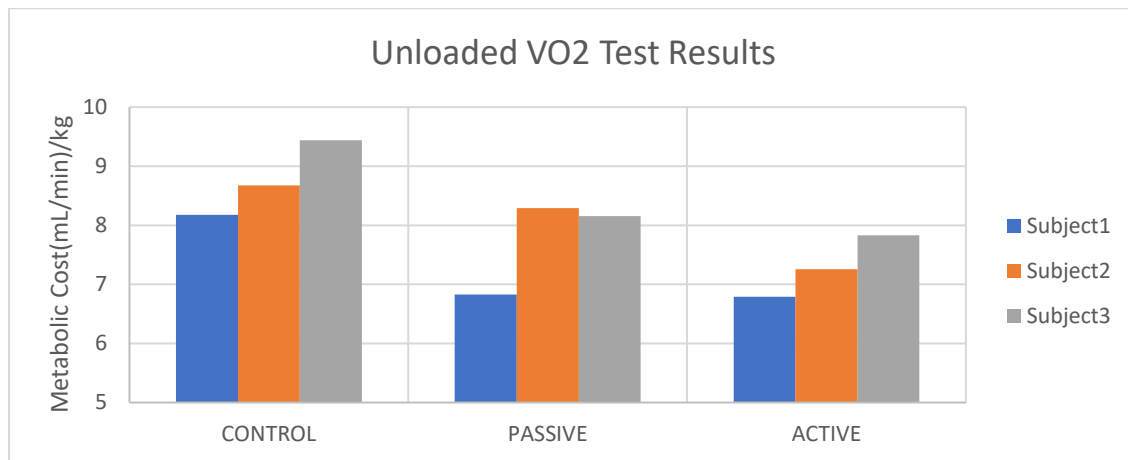


Figure 20 Results from VO2 Squat Testing without External Load for Three Subjects.
Note: the vertical axis range has been selected from 5 ml 〖min〗^(-1) kg^(-1) to 10 ml 〖min〗^(-1) kg^(-1) to better illustrate the differences in result values.

Figure 20 shows the results of the unloaded LCPS tests. The A-LCPS is shown on the right to have the most significant reduction in VO2. The results indicated that P-LCPS did show a decrease in metabolic cost but was not as consistent as the A-LCPS.
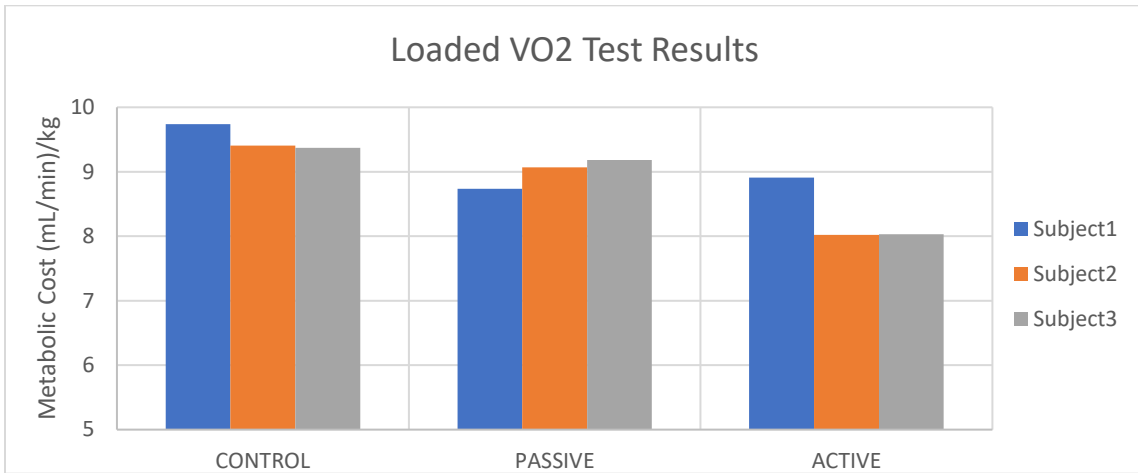
Figure 21 Results from VO2 Squat Testing with External Load for Three Subjects.
Note: the vertical axis range has been selected from 5 mL 〖min〗^(-1) kg^(-1) to 10 mL 〖min〗^(-1) kg^(-1) to better illustrate the differences in result values.

Figure 21 illustrates the loaded VO2 test results where the test subjects were handed masses equal to 10% of their body weight while squatting. According to this data, there is still a reduction in both suits' metabolic costs, but the results are less substantial than those of the unloaded squatting test.
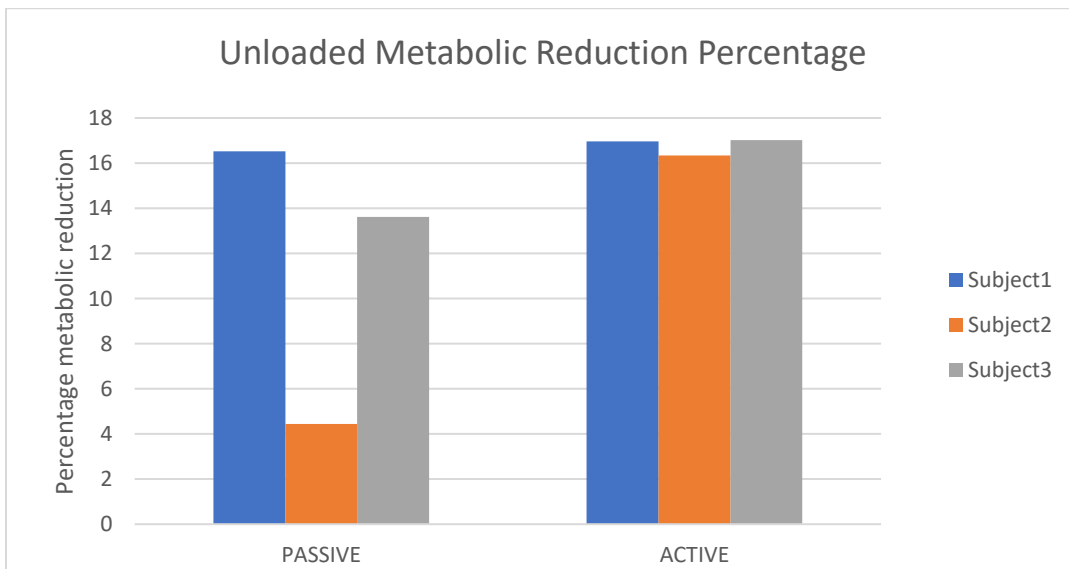


Figure 22 Comparison of Passive and Active Versions of the LCPS Using Metabolic Cost Savings as a Percentage to Quantify the Effect. The Vertical Axis Indicates the Percentage of Energy Saved Compared to that of a Control Test with No Assistive Device.

33
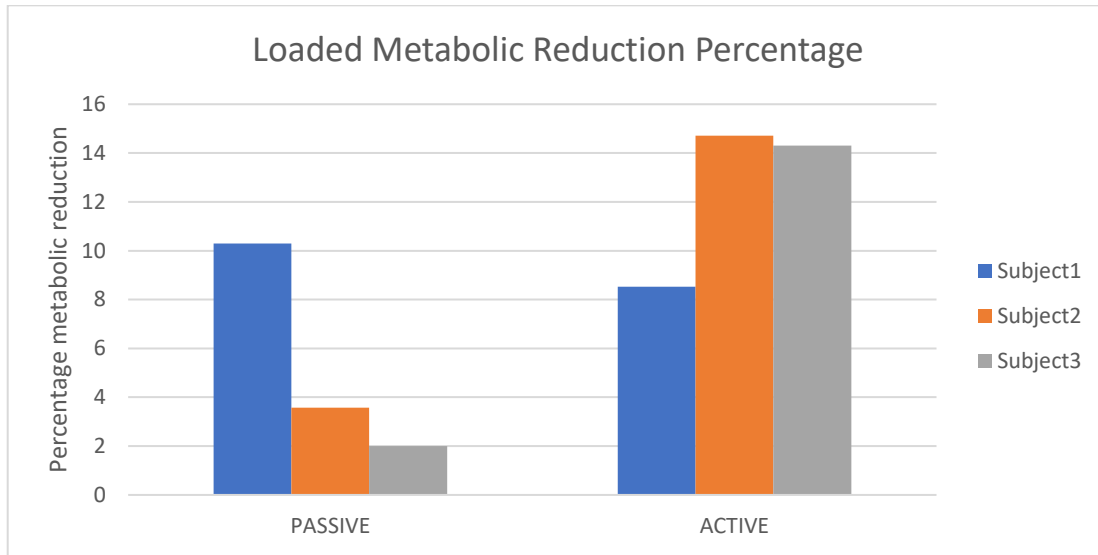
Figure 23 Comparison of Passive and Active Versions of the LCPS Using Metabolic Cost Savings as a Percentage to Quantify the Effect.

Figure 23 shows the same data from the squatting tests organized in terms of metabolic reduction as a positive percentage. Note that the positive percentage indicates a metabolic decrease in energy when compared to the control. The vertical axis indicates the percentage of energy saved compared to a control test with no exoskeleton.

3.5. Conclusion

This chapter covered a squat assisting exoskeleton's design and development that actively avoided undesired knee resistance. The chapter also included the testing procedure and data, which compared its performance to a similar passive design. The data collected revealed an 11.5% reduction in metabolic cost for squatting with the P-LCPS with no extra load and a 5.3% reduction in the loaded condition. For the A-LCPS, the data suggests a roughly 16.7% reduction in metabolic cost in the unloaded state and a 12.5% reduction in the loaded condition. A significant aspect to note in this comparison is the weight of each exoskeleton. The P-LCPS weighs approximately 2.86 kg, whereas the A-LCPS weighs approximately 5.76 kg. The results indicate that although the P-LCPS exoskeleton weighs roughly half that of the A-LCPS, the metabolic cost reduction level is more significant for the A-LCPS. The results were likely due to the practice of allowing each subject

to set their level of tension for each exoskeletons' bungees. Although this has not been confirmed, the bungee used on the A-LCPS could be more comfortably worn at a higher tension since walking resistance was not increased proportionally to the bungee's tension as was the case for the P-LCPS.

## 4 DESIGN OF AN ACTIVE ANKLE FOOT ORTHOSIS FOR GAIT ASSISTANCE

4.1. Background

This chapter covers the design and testing of an Active AFO (AAFO) exoskeleton developed to provide anterior-posterior ground reaction force for gait assistance. The finalized AAFO prototype for gait assistance was capable of pneumatically-powered dorsiflexion and plantar flexion. It was similar to the design by (Ferris, Czerniecki, & Hannaford, An Ankle-Foot Orthosis Powered by Artificial Pneumatic Muscles, 2005), with a few key differences. The powered AFO by Ferris et al. used carbon fiber leg and foot attachments made using custom plaster molds from the subject's leg, with titanium fittings (Ferris, Czerniecki, & Hannaford, An Ankle-Foot Orthosis Powered by Artificial Pneumatic Muscles, 2005). Conversely, this research has taken an economical approach to its construction as the AAFO developed instead used primarily inexpensive components, many 3D-printed with common material, with a quasi-universal fitment not tied to a specific user. Additionally, the AAFO described in this research does not lock the ankle joint in the sagittal plane as is done with many other AAFOs. This economical and practical design seeks to address many competing AAFO devices' prohibitive costs and produce increased anterior-posterior GRF for those in need of gait assistance.

4.2. Design

For actuation, a pneumatic cylinder was used to allow for a range of resistive and assistive forces depending upon the applied pressure and to which port it is applied. This level of control is necessary to accommodate subjects with varying degrees of mobility, aiding their progression toward recovery in a quantifiable way. Design goals for the device included being unobtrusive, cost-effective, easy to wear, and active. The AAFO prototype's design had undergone progressive changes from its original configuration; however, the device's core principles and mechanical configuration have remained the same throughout. The AAFO was designed and modeled using SolidWorks Computer-Aided Design (CAD) software. A CAD model of the initial AAFO prototype assembly can be seen in Figure 24.
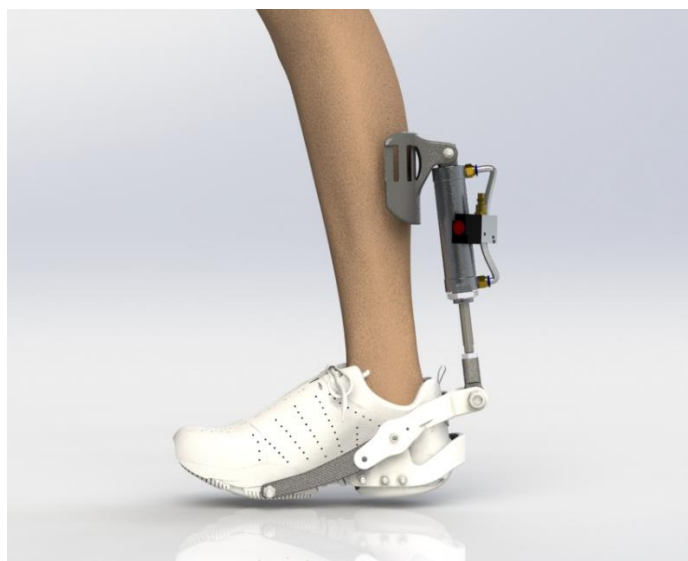
Figure 24 CAD Model of AAFO Assembly.

The design used an arm that pivoted about the ankle joint, applying forces through the shoe to the ground rather than acting directly on the user's foot. The user's shoe would require only slight modification in the form of eight small screw holes in the shoe's sole where the AAFO is secured. In this way, there would be minimal weight added to the user's leg(s), and a range of shoe sizes could be accommodated with minor modification. As a result, there would be no requirement for custom-fitted orthotics, which could be both costly and time-consuming. The ankle attachment was adjustable to suit a range of lower-leg sizes. The prototype was primarily composed of 3D-printed parts with commercial steel or aluminum hardware connecting them. An early design was assembled and tested in a gait lab where kinematic and force plate data was collected and used to determine the supplemental ankle power while walking. Although future versions of the AAFO were powered, the first version of the AAFO to be tested would be non-powered, as shown in Figure 25.
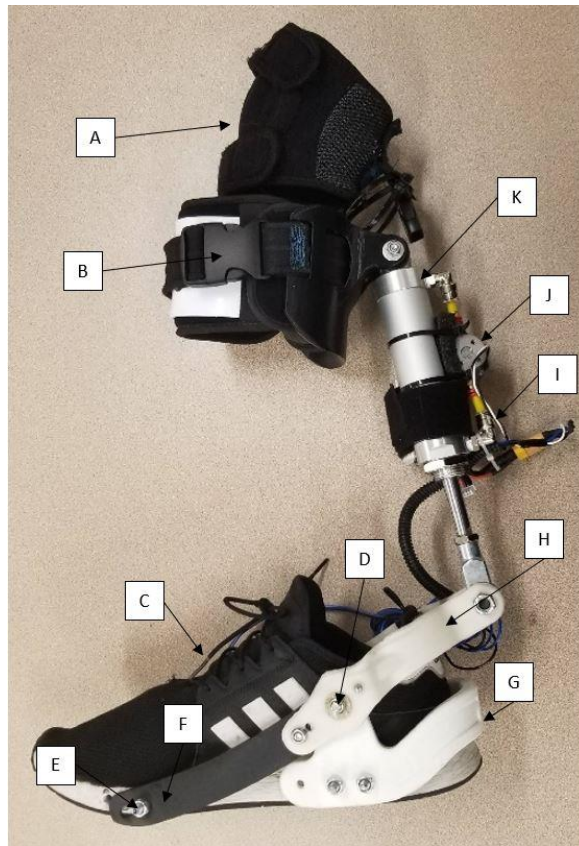
Figure 25 Non-powered AAFO Prototype Assembly Image.
A – Knee Brace, B – Shin Attachment, C – Shoe, D – Pivot Joint, E – Front Shoe Attachment, F – Bump-Switch (Location), G – Rear Shoe Attachment, H – Leverage Arm, I – Lipo Battery, J – Two-Way Air Solenoid Valve, K – Double-Acting Air Cylinder.

The prototype AAFO seen in Figure 25 was tested to investigate its effect on walking gait in a non-powered configuration. This non-powered version was intended to work in essence as a pneumatically controlled spring, where the air cylinder would be actively closed from the "Foot Flat" phase of the gait cycle (roughly 10%) up until the "Toe Off" phase (at approximately 60%) of the gait cycle. An illustration of the gait cycle can be seen in Figure 26.
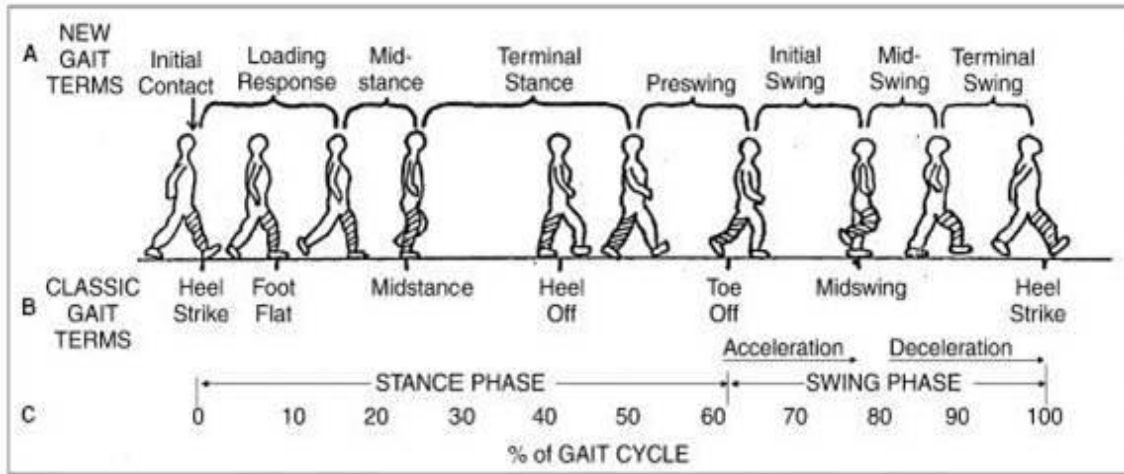
Figure 26 Gait Cycle Illustration with Percentages (Gait, n.d.)

Control of the non-powered AAFO was achieved by using a bump-switch fixed to the forward-most part of the AAFO. The switch had been activated by toe contact with the ground, which would activate a pneumatic solenoid connecting the upper and lower chambers of the double-acting cylinder.



Figure 27 AAFO Switch-Controlled Prototype Un-Powered Test Image.

The non-powered AAFO test was performed with a single healthy male subject with the device on one foot and a standard running shoe on the other, as seen in Figure 27. A motion capture system was used to collect kinematic and GRF data of the subject over three minutes of walking at 1m/s. A control test was also performed by the same subject under the same conditions, only with typical running shoes and no exoskeleton.
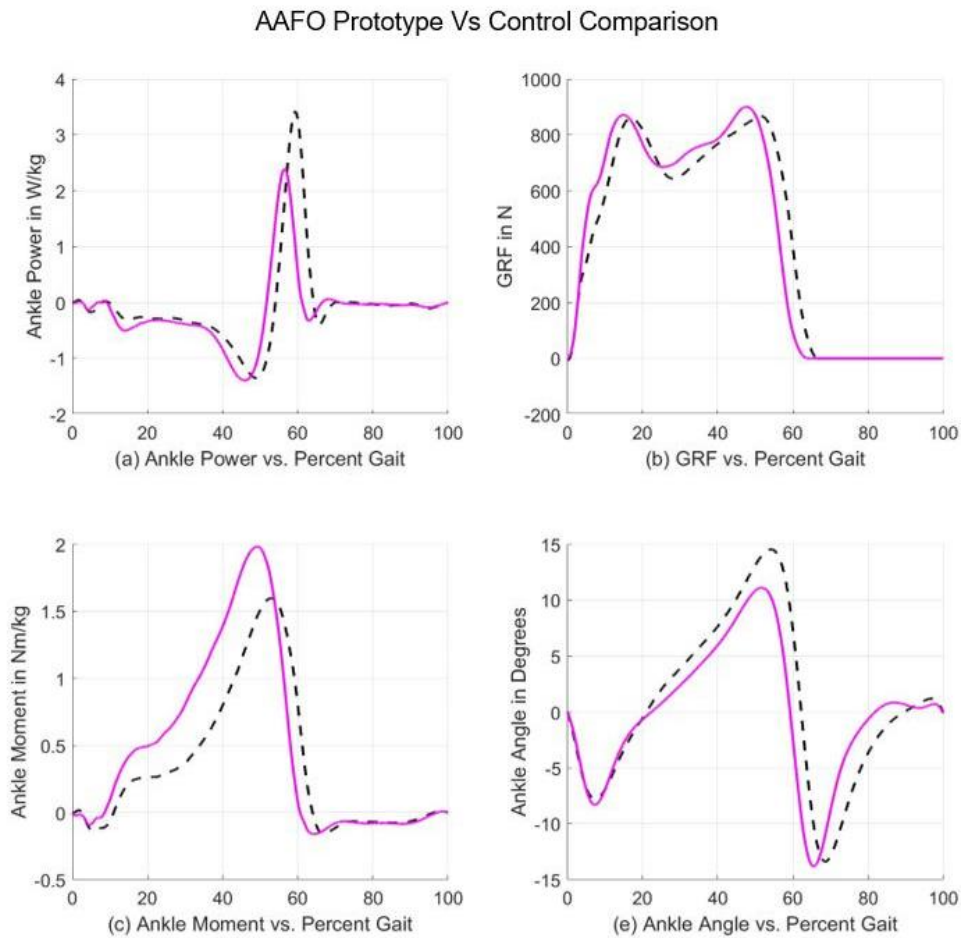


Figure 28 Kinematic Data Comparison of Walking Gait at a Speed of 1m/s on a Healthy Subject with Typical Running Shoes vs. the AAFO Configured as a Pneumatic Spring.

The test results shown in Figure 28 illustrate the comparison between the AAFO and the control test. The dashed line shows the control results, and the solid line represents that of the results with the AAFO attached. The results seemed to indicate that un-powered AAFO performed

poorly as a device for assisting in walking gait, as ankle power was reduced. One possible contributing factor may have been a lack of sufficient time for the subject to become acclimated to wearing the AAFO prototype before performing the test. Another possible contributing factor was the weight of the AAFO requiring greater inertia for push-off motions, negating the actuator's positive effect. The results indicated that a powered configuration of the AAFO might be more successful. Following the unsatisfactory results from the un-powered configuration of the AAFO, modifications were made to reconfigure it into a powered AAFO which would be supplied with compressed air. Changes were made to the feedback system and air system to accommodate the transition.

The first configuration of the AAFO was controlled using feedback from bump switches that would contact the ground. The pneumatic double-acting cylinder attached parallel to the subject's Calcaneal (Achilles) tendon acted as a pneumatic spring, storing energy and releasing it while walking. The powered AAFO would be capable of providing greater supplemental assistive forces to aid a subject in rehabilitation. It would use the same double-acting pneumatic cylinders for actuation and the same basic mechanical structure as the non-powered AAFO prototype. Unlike the non-powered AAFO however, IMUs would be used to provide feedback and determine the point of actuation instead of using bump switches. The system detects the user's leg in motion by using the Euler angles in the sagittal plane (i.e., a longitudinal anatomical place that divides a human body into left and right parts) obtained from IMU sensors, which are also attached to the front of the user's shank.

4.2.1. Mechanical System Design

The powered AAFO's design takes a mechanical approach to supplement the Soleus and gastrocnemius muscles in a controlled manner while allowing for the maximum range of motion and comfort of the user. Just as with the non-powered version, the powered design offers reasonable accommodation to a variety of users with respect to shoe size and weight and can be quickly adjusted such that it does not reduce the range of motion of the ankle. Adjustments are

41

made by replacing the lever arm such that it is aligned to the ball of the foot and by tightening or loosening the newly added turnbuckle connecting rods. These adjustments allow the AAFO to operate at up to approximately 25 degrees of dorsiflexion and up to approximately 70 degrees of plantarflexion. The connecting rods were necessary to remove the need for a knee attachment, drastically reducing any chafing issues which resulted from movement of the shank attachment in the non-powered prototype. The connecting rods use swivel-ball ends, which allow some degree of foot rotation as well as inversion and eversion of the foot. The dorsiflexion and plantarflexion angles can be seen in Figure 29. The powered AAFO shoe attachment method was unchanged, using eight self-tapping screws to secure it to a range of both styles and sizes of running or walking shoes, maintaining the intended user comforts, affordability, and accessibility.
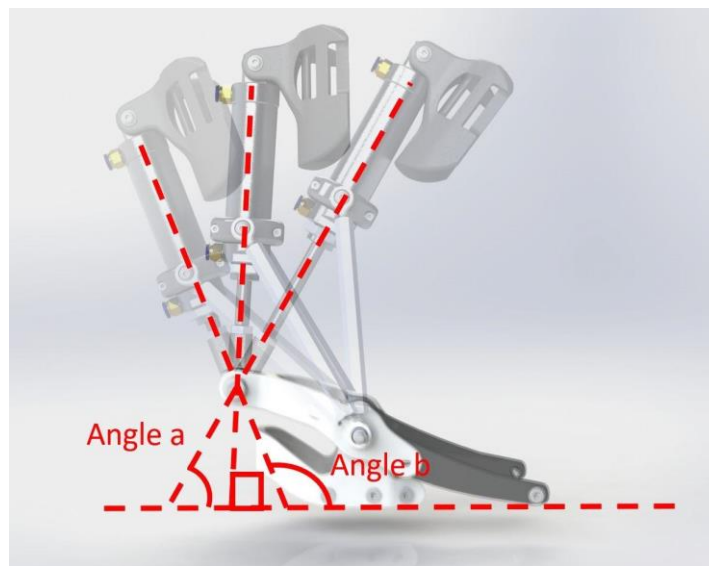


Figure 29 Maximum Variation of Angle for Plantar- and Dorsi-flexion

Illustrated in Figure 29, the powered AAFO used a lever arm free to pivot in the middle around a steel pin and was fixed to the fore-end of the user's shoe. The arm's pivot point is secured to the hind end of the user's shoe, and the other end of the lever arm is attached to the double-acting air cylinder where retraction and extension forces were applied. Geometric relationships could be used to derive the relationship between input air pressure and maximum theoretical propulsive force.

Equation 1 Ground reaction force equations

$$F_{GR} = cos(\theta) \times P_{air} \times A_{cylinder} \times \frac{d_1}{d_2}$$

$$F_{GR} = cos(\theta) \times P_{air} \times 5.34$$

The application of the force on the mechanical parts of the design can be seen in Figure 29. The equation above can be used to calculate the maximum theoretical propulsive force of the AAFO. With a cylinder bore of approximately 32mm and a maximum pressure of approximately 70 psi, the maximum theoretical force the AAFO can provide is approximately 287.28 N. Using 4.25mm inner diameter hoses, approximately 1.37 m in length from the air solenoid, the response time of the actuator system is approximately 0.104 seconds. This is a limiting factor for the system in terms of user agility, as it is not suitable for typical human running speed. However, human agility in terms of terrain angle should not be limited by the device, as it offers a high degree of abduction, adduction, inversion, and aversion. To minimize the weight being added to the lower extremities, much of the system's pneumatics were relocated remotely to reduce the adverse metabolic effects of increased weight to the lower legs. A Condor Modular Operator Plate Carrier (MOPC) was used to house the pneumatic control equipment for the suit, including the air solenoids, batteries, and all electronics except for the sensors and the AAFOs themselves. The Air solenoids used were Numatics 236127B 24V 6Watt Solenoid valves and were responsible for controlling the airflow through the system. The sensor casings and much of the AAFO parts except for the air cylinder and hardware were 3D printed in polylactic acid material. The double-acting air cylinder used was a Sydien Single Rod Double Action Pneumatic Cylinder with a 32mm bore and a stroke of 75mm.
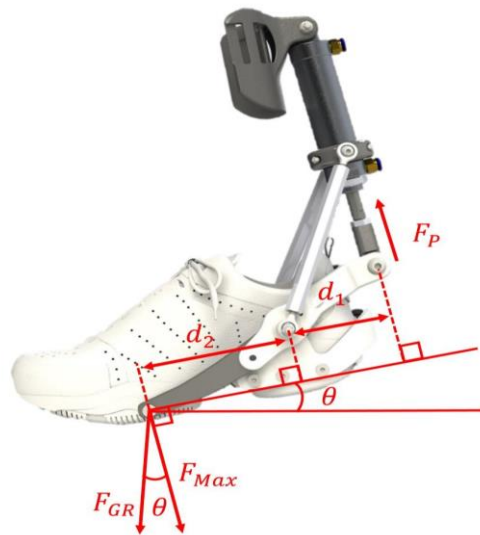
Figure 30 Geometric Representation of the Force Acting on the AAFO.

Air was supplied via a commercial air compressor located remotely. A mobile air supply system would have been similarly effective at delivering propulsive force and was successfully tested as a proof of concept. The portable air supply system can be seen in Figure 31.
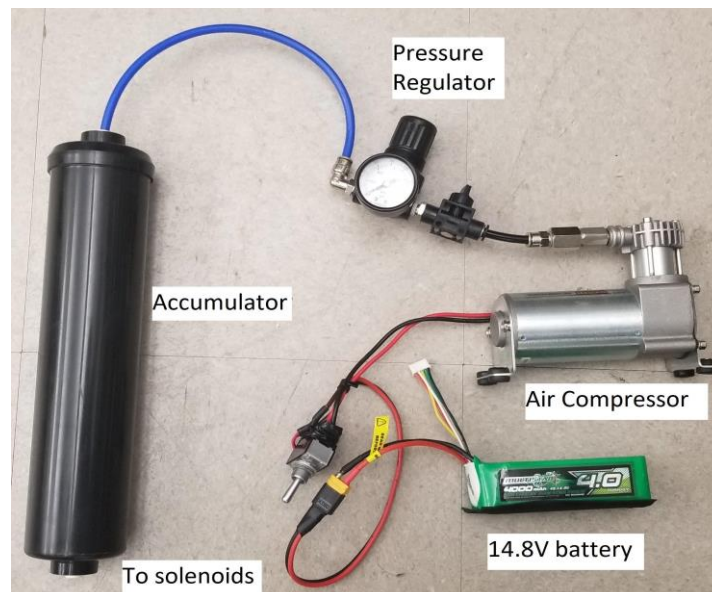


Figure 31 Mobile Air Supply with Accumulator and Pressure Regulator.

The lever arm's design and orientation, linkage arms, and shank support work together to provide a rigid connection between the shank and foot with minimal chafing or rubbing. The air cylinder contracting force is transferred through the level arm to the front of the foot, where the foot typically reaches maximum Plantar flexion at the beginning of the swing phase, ensuring maximum propulsive force duration.

4.2.2. Electronic System Design

The AAFO uses an Adafruit Feather HUZZAH with ESP8266 processor onboard to process and transmit the incoming IMU data for data analysis on computers via WiFi and output control signals to two VNH5019 motor driver carriers. The motor drivers are responsible for activating the air solenoid valves and thus control the pneumatic actuation of the AAFO. The IMUs used are two Adafruit (Adafruit Industries, New York, NY) BNO055 absolute orientation sensors placed on the shank of the subjects using straps and custom-designed sensor housing. The paper from Quintero et al. (Quintero, Lambert, Villarreal, & Gregg, 2017) showed a similar application of using IMU sensors for detecting gait cycles for lower orthotics. The feather Huzzah is programmed using the Arduino IDE, and a MATLAB (Mathworks, Natick, MA) script was developed to acquire the data via WiFi remotely. The IMU sensor is a 9-DOF sensor with a 3-axis accelerometer, gyroscope, and magnetometer.

4.2.3. System Block Diagram

Figure 32 illustrates the workings of the AAFO system as a block diagram. The $V_1$, $V_2$, $V_3$, and $V_4$ are the solenoid valves that control the two cylinders' actuation. The IMU's communicate with the Microcontroller on the I2C (Inter-Integrated Circuit) communication bus with clock and data lines. There is an internal 10k pull-up resistor on the IMU board to provide the signal lines' default states.

45
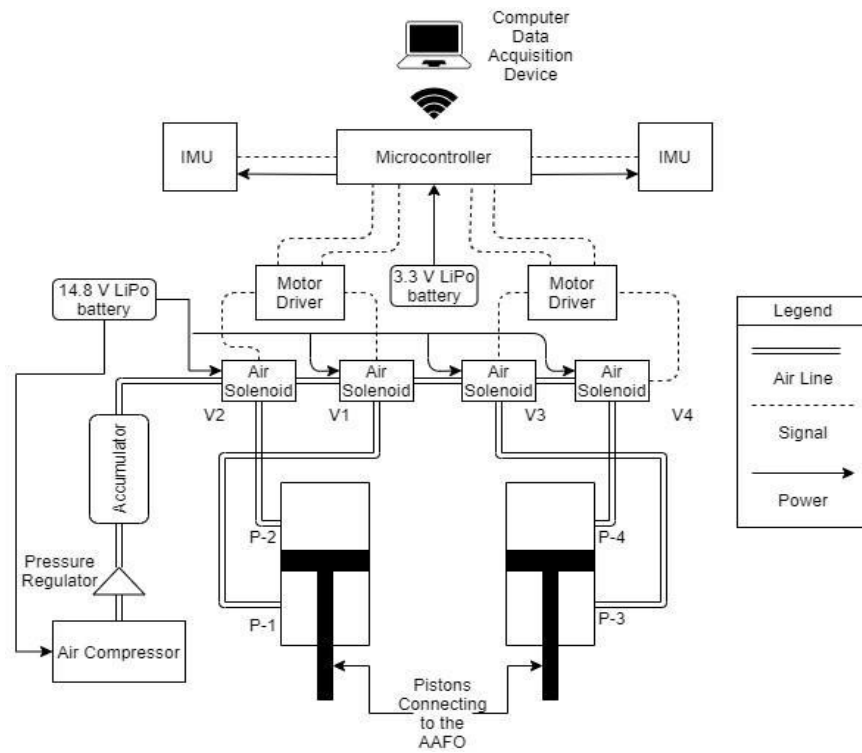
Figure 32 Block Diagram of Basic Air and Electrical System of the AAFO.

### 4.2.4. Control Algorithm

Algorithm 1 was designed for controlling the actuation of the cylinder based on the Euler angle inputs from the IMU sensors. The $V_1$, $V_2$, $V_3$, and $V_4$ are the solenoid valves shown in Figure 4. The connection diagram mentioned in (Qi, Bone, & Zhang, 2019) was used for finalizing the solenoid connections. The control parameters defined in the algorithm are described as follows: - $\alpha$ is the threshold angle for the absolute difference of the angles between the two IMUs. $\alpha_1$ is the left shank angle, and $\alpha_2$ is the right shank angle with respect to the vertical plane from the sagittal side. $\lambda$ is the flag that determines which leg needs to be actuated. It is set to 1 left leg and 2 for the right leg. This ensures that a single leg is not actuated consecutively during a single gait cycle. $\tau$ is the time delay for the sensor read. This was set to the minimum amount possible for consistent data communication over Wi-Fi for the data acquisition system. $t_0$, $t_1$, and $t_2$, are time set for determining the various phases of the gait cycle. Since the experiment was conducted at a constant speed, the values remained constant throughout the experiment.

46

---

**Algorithm 1** Control algorithm for the device

---

**Initialize**: Sensor system, Wi-Fi module, calibration parameters, control parameters like $\alpha$, $\lambda$, $\tau$, $t_0$, $t_1$ and $t_2$. Obtain offset values from calibration parameters for the
sensors
**while** Client connected **do**
　Obtain $\alpha_1$ and $\alpha_2$ from IMU sensors {Retrieve the Euler angles from IMU sensors}
　**if** $abs(\alpha_1-\alpha_2) > \alpha$ **then**
　　**if** $\alpha_1 < \alpha_2$ and $\lambda \sim= 1$ **then**

　　Activate $V_1$ {Extend Left leg for push off}
　　Start counter $t = t_1$
　　Set $\lambda = 1$ {Here *lambda* = 1 indicates left leg}
　　**else if** $\alpha_1 > \alpha_2$ and $\lambda \sim= 2$ **then**
　　Activate $V_3$ {Extend Right leg for push off}
　　Start counter $t = t_1$
　　Set $\lambda = 2$ {Here *lambda* = 2 indicates right leg}
　　**end if**
　**else**

　　Deactivate $V_1$, $V_2$, $V_3$ and $V_4$ {Free move state}
　　**end if**
　　Reduce counter $t$
　　**if** $t < t_2$ **then**
　　　**if** $\lambda = 1$ **then**

　　　Activate $V_2$ {Retract Left leg for heel strike}
　　　**end if**
　　**if** $\lambda = 2$ then

　　　Activate $V_4$ {Retract Right leg for heel strike}
　　　**end if**
　**end if**
　wait for $\tau$ ms {Delay for sensor read}
**end while**

---

Figure 33 Algorithm for AAFO Control

　　　Figure 33 shows the various phases of a single gait cycle as captured from the testing of

the device by the subjects. The nomenclature of each phase was obtained from (Taborri, Palermo,

Rossi, & Cappa, 2016). Here, the phases are labeled according to the subject's left leg (i.e., the leg closer to the camera). The angle $\alpha$ is the angle difference between the two IMU sensors placed in front of the shank of the subject. The sensors provide the shank angle on the sagittal plane of the subject. Here $\alpha$ is the control parameter used in control algorithm 1. The shank angle measurements were calculated using the method shown in Figure 33. In the paper (Watanabe, Saito, Koike, & Nitta, 2011), the angle variation of the knee for each phase of the gait cycle is shown, and by using those values, the timings for the actuation of the cylinders were estimated. The estimated values were confirmed with the IMU sensors' data, as shown in Figure 33 by observation during the habituation phase of the subjects to determine the values for the control parameters $\alpha$, $t_0$, $t_1$, and $t_2$. These values were also adjusted according to the comfort of the subjects.

4.3. Results and Discussion

### 4.3.1. Testing Procedure

After IRB approval, a preliminary test of the device was conducted to determine its ability to provide assisted plantar flexion. Four subjects were tested on an instrumental dual-belt treadmill with force sensors (Bertec, Columbus, Ohio). The subjects were fitted with the device on both of their legs and were made to wear the condor plate carrier with all the additional equipment. The testing phase had two sessions.

Habituation Test for acclimatization to the device: In their first session, the subjects were fitted with the AAFO and were made for walking on the ground for 5 minutes to habituate themselves with the device. They were given 10 minutes on the treadmill with varying speeds between 0.5 m/s to 1.2 m/s to acclimate themselves to the shoes for the final testing session. During their habituation time on the treadmill, data of their shank angle variation was collected from the IMU sensors for estimating their plantar flexion time and their swing phase time for synchronizing the actuation of the cylinders. The source pressure varied from 30 psi to 70 psi and the subjects were notified about the pressure before to allow them to anticipate the assistance from the device.

48

Walking test for collecting ground reaction force: In their second session, the subjects were instructed to walk on the treadmill for 1 min with both legs split on the right and left a belt of the treadmill with a regular walking speed of 1 m/s. A passive reflective heel marker was placed on both the heels of the subject to determine the heel-strike event on the treadmill. The motion of the heel marker was captured using a motion capture system (Vicon Nexus 2.0, Computer Software, 2020) at 1000 Hz. There were four pressure conditions used for testing the ground reaction force: 1) No pressure, 2) Pressure at 30 psi, 3) Pressure at 50 psi, 4) Pressure at 70 psi. Ground Reaction Force (GRF) was collected for each of the pressure used. Healthy subjects of a similar age group without any impairments were used for the test. Subject information can be found in Table 1.

4.3.2. Results

Figures 7,8,9 and 10 represent the Anterior-Posterior GRF obtained from the left leg of the 4 subjects. The initial data from the motion capture system was processed in the Vicon Nexus software (Vicon Nexus 2.0, Computer Software, 2020), where the markers were labeled, and gaps were filled with a custom plugin.

Table 1 Test Subject Attributes

| Attributes | Sub A | Sub B | Sub C | Sub D |
|---|---|---|---|---|
| Height(cm) | 177.8 | 172.2 | 177.8 | 185.4 |
| Weight(kg) | 88.45 | 87.54 | 87.99 | 112.35 |
| Age | 20 | 25 | 25 | 25 |
| Shoe size (US) | 11.5 | 9.0 | 9.5 | 12.0 |

The data was then extracted and further processed on MATLAB software (MATLAB. Version 2018a, Computer Software, 2018). The raw data was initially filtered with a 2nd order low pass Butterworth filter of 10 Hz. The heel strike events were calculated by finding the recurrence of the least angle of the heel marker. The individual gait cycles were then extracted from the filtered data, they were then curve fitted to match the dimensions, and an average of 5 gait cycles were taken to

obtain the average plots. The plots show the GRF obtained for the four pressure conditions. The

red line indicates the GRF at 0psi, the green line indicates GRF at 30psi, the blue line indicates

GRF at 50psi, and the black line indicates GRF at 70psi. The GRF data of Subject D at 70psi was

a flawed trial and was excluded from the plots. The initial trough in the plots is the Braking force

applied by the stepping leg to go from the gait cycle's swing phase to the stance phase after heel

strike. The peak that follows from the trough represents the Propulsive force that the stepping foot

generates to transfer from the stance phase to the swing phase of the gait cycle.
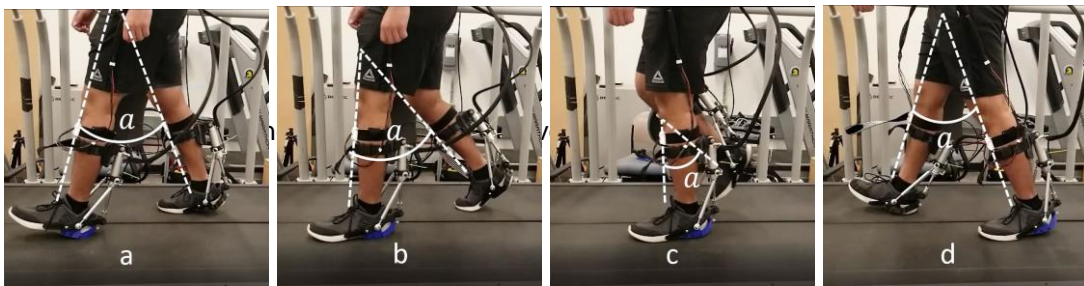


Figure 34 A Single Gait Cycle with 8 Levels of Granularity.
(a) Double support, Heel Strike (b) Single Support, Loading response (c) Single Support, Mid stance (d) Single Support, Terminal stance.
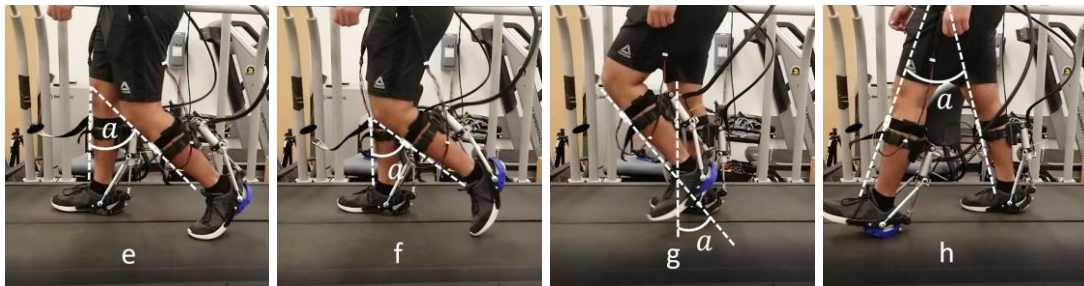


Figure 35 A Single Gait Cycle with 8 Levels of Granularity (cont.).
(e) Double Support, Pre Swing (Push-off) (f) Single Support, Toe-off (g) Single Support, Mid Swing (h) Single Support, Terminal Swing.

4.3.3. Analysis

The results from this preliminary testing of the device show a higher GRF during propulsion,

with an increase in supply pressure added to the cylinder. For this experiment's purpose, only the

left leg GRF was analyzed; however, during the experiment, the subjects were wearing the device

on both legs to induce symmetry. This trend of increasing GRF with an increase in force is attributed to the force applied to the ball of the foot by the device during push-off. The additional push-off force increased the anterior-posterior propulsion of the stepping leg. The results from subject A in Figure 37 show that the highest increment of GRF from the powered-off condition was when a pressure of 30 psi was applied. Subject A revealed during the post-session that it felt the most comfortable with 30psi pressure. Subject B, C, and D all expressed that they could feel a higher push-off force with the increase in pressure. Subject A had a variation between 34.87% to 25.43% increase in GRF for the three different applied pressures. Subject B showed a variation between 6.5% to 47% increase in GRF for the different pressures. Subject C showed a variation between 82.44% to 89.61% increase in GRF with the different pressures. Subject D showed a variation of 42.4% to 116.8% increase in GRF with different applied pressures. Different control parameters were used for different subjects, which could have been attributed to the propulsion force peaks' high variation.
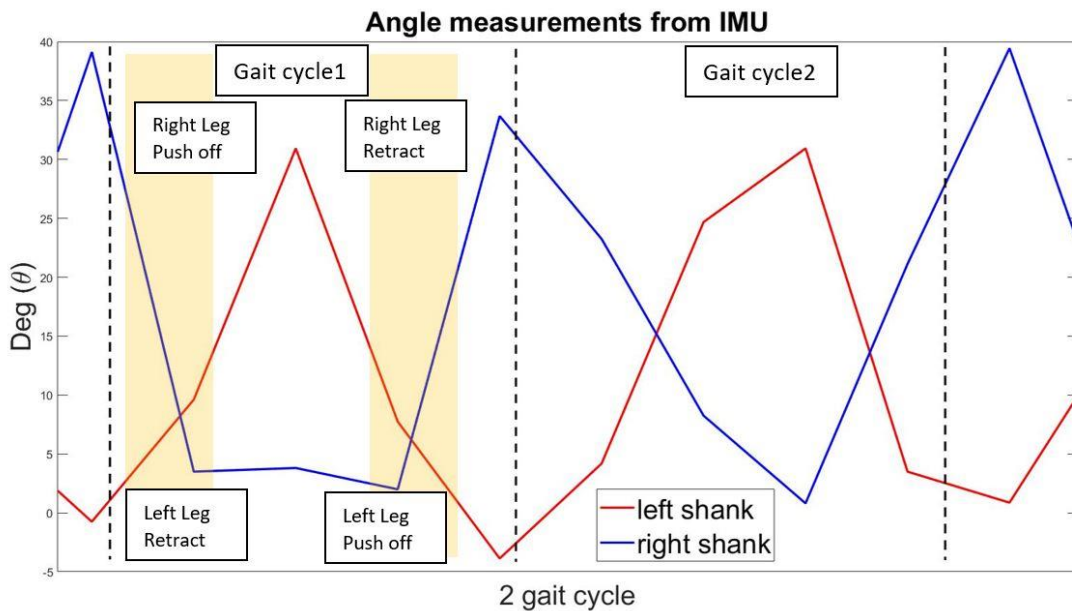


Figure 36 Shank Angle Measurement from IMU Sensors
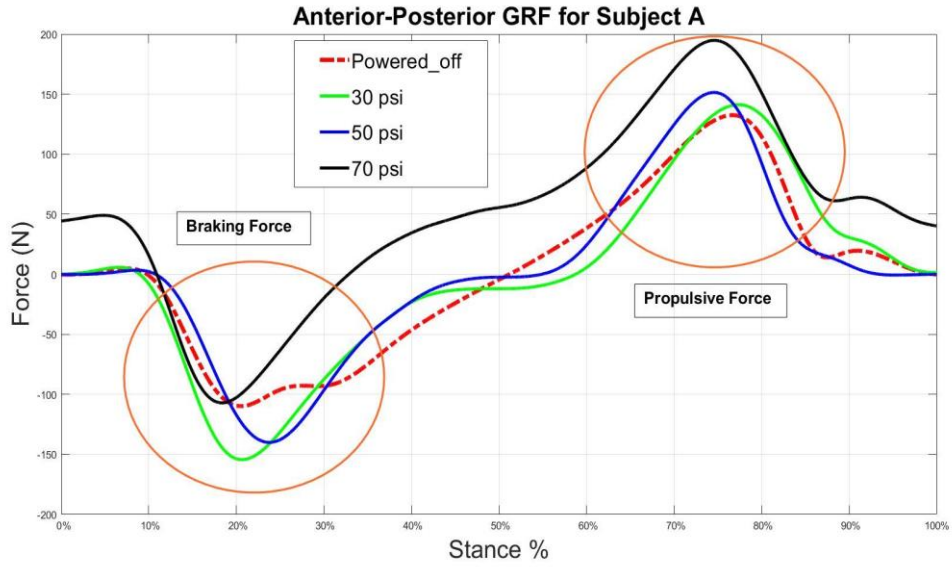
Figure 37 Anterior-Posterior GRF of the Left Leg of Subject A.
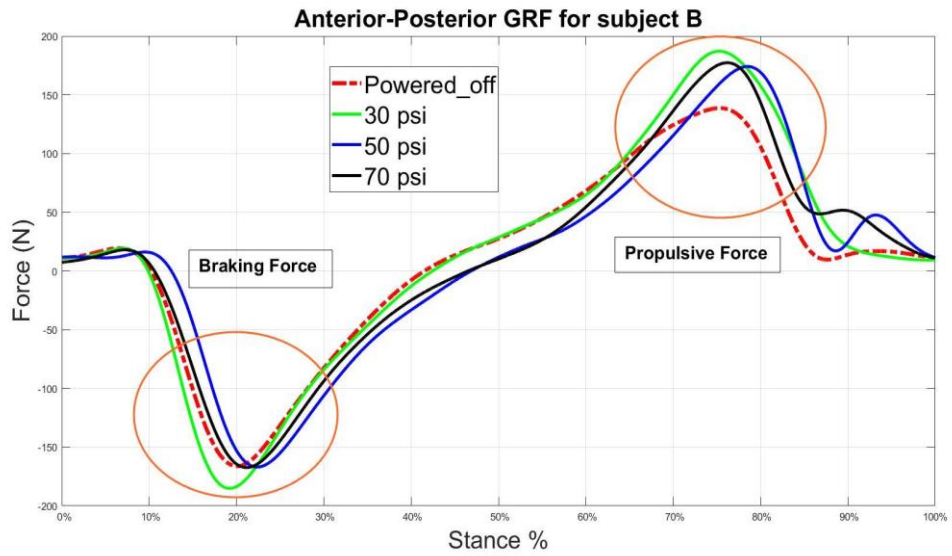


Figure 38 Anterior-Posterior GRF of the Left Leg of Subject B.
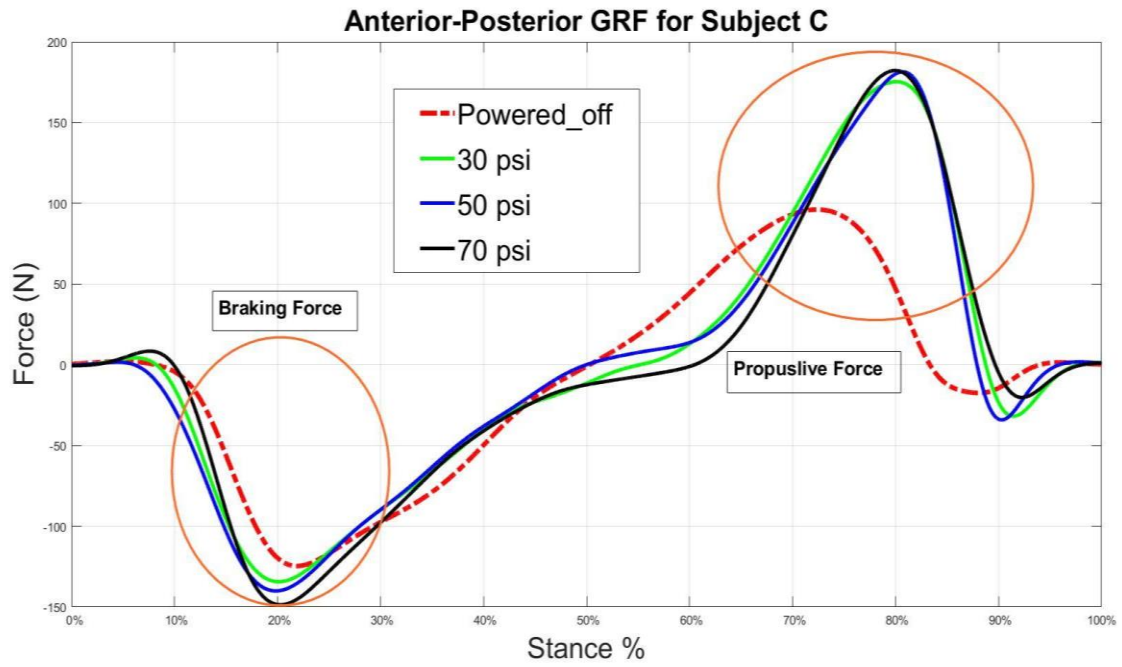
Figure 39 Anterior-Posterior GRF of the Left Leg of Subject C.
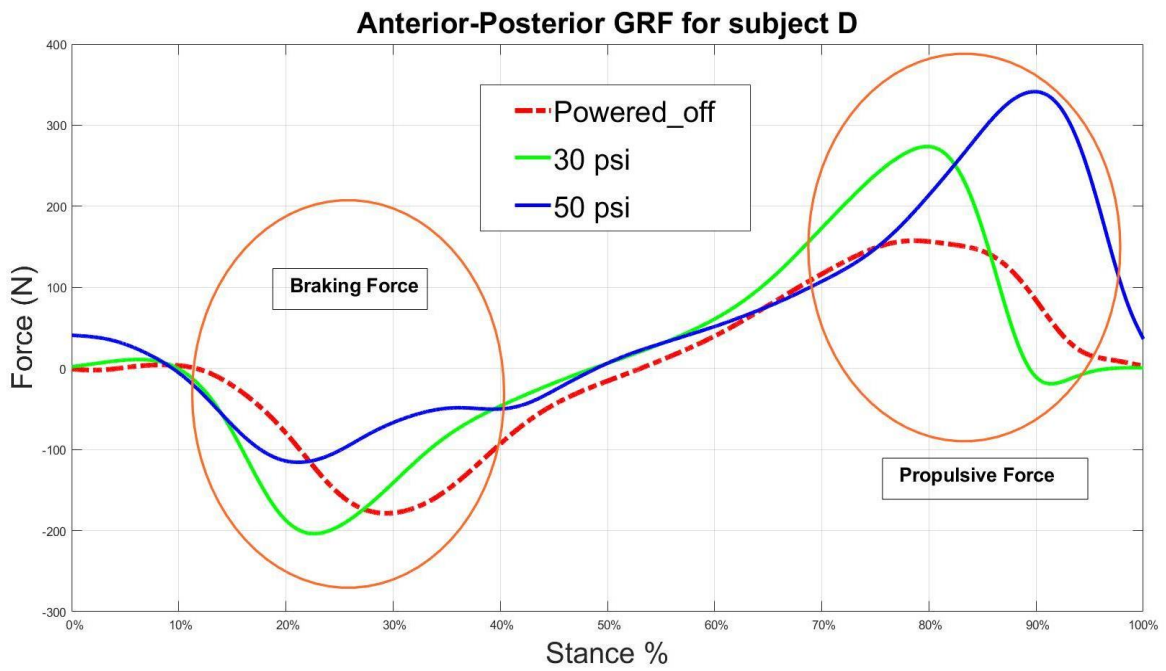


Figure 40 Anterior-Posterior GRF of the Left Leg of Subject D.

4.4. Conclusion

This chapter covered the design and testing of an AAFO capable of increasing the user's ground reaction forces while being cost-effective and comfortable to wear. For those in need of gait assistance, the device described offers a platform that could be built upon to aid in gait therapy and rehabilitation exercises. For those who have suffered from a stroke and have a higher risk of falling, there is evidence that an active ankle-foot orthotic device can provide a strong plantarflexion to the ankle, mitigating the factors that cause them to fall. The design of this device utilizes easy-to-use components and a custom algorithm to provide a stronger push-off during normal gait, such that the individuals wearing the device would be able to generate a stronger ground reaction force. Evidence from other studies suggests that a stronger ground reaction force would help in better forward propulsion and would help individuals take faster compensatory steps in the event of a fall. Preliminary tests on 4 subjects showed a general trend of an increase in the anterior-posterior ground reaction forces in the powered condition. There is a need for comprehensive testing of the device to fine-tune the control parameters and make it a useful tool for gait assistance and possibly fall prevention.

## 5 DESIGN OF AN ACTIVE ANKLE FOOT ORTHOSIS FOR FALL PREVENTION

### 5.1. Background

This chapter covers a further reconfigured design of the powered AAFO exoskeleton that applies an assistive force at the heel to improve push-off using soft actuation. This soft-actuated configuration of the AAFO was designed with the intent of use for fall prevention and is similar to the orthosis in (Gordon, Sawicki, & Ferris, 2006). Gordon et al. were concerned with the length of their actuators and the type of force being applied. In contrast, this research has sought to investigate the timing and pressure value combinations for actuation using an economical and quasi-universal fitment AAFO device that doesn't constrain the user's ankle to the sagittal plane. The research in (Polinkovsky, Bachmann, Kern, & Quinn, 2012) also explored a similar orthosis that used SEAs. Their orthosis was deemed sufficient to prevent drop foot but did not comment on its capability to improve push-off.  This article delves into when to apply the force and the relationship between the force applied and timing. A force needs to be applied during push-off. However, the details of what instance to apply the force were unknown to the best of the author's knowledge. The current article has conducted experiments to determine the best time to apply an assistive force to aid plantarflexion/ push-off.

To improve push-off, one needs to apply the right amount of force (or moment) at the right amount of time for the right amount of time. After push-off, the exoskeleton should be out of the way and not obstruct motion. A successful exoskeleton combines innovative hardware design coupled with smart control strategies to personalize the robot to the user. This chapter presents the hardware design, control strategies, and testing results for the AAFO. The preliminary results show improvement in propulsive force and a reduction in muscle activity. The AAFO design allows inversion, eversion, external and internal axial rotation. It is comfortable to wear and easy to DON-DOOFF.

5.2. Design

The primary design goal of the AAFO prototype was to increase propulsive GRF without constraining their ankle movement to the sagittal plane (as seen in (Gordon, Sawicki, & Ferris, 2006)). The prototype was designed to fit a large user population. The device was made detachable. A shank attachment was provided, which was adjustable to accommodate different users. The mechanical components of the AAFO can be seen in Figure 41.

5.2.1. Design

The prototype was primarily constructed out of 3D-printed Polylactic Acid (PLA) plastic. Aluminum turnbuckles with steel tie-rod ends were used to connect the upper and lower assemblies. A commercial soft pneumatic artificial muscle (PAM) and commercial tactile switches were incorporated for feedback and actuation. These switches were used to detect gait phases in the past (Taborri, Palermo, Rossi, & Cappa, 2016). The design featured a vertically adjustable shank mounting that could be adjusted by rotating the turnbuckles on either side of the AAFO, shown in Figure 41. The AAFO can be attached to the users' shoes using straps. Non-elastic straps were used to fix the upper and lower shank braces to the user's lower legs, as seen in Figure 41. Ball joints on either end of the adjustable turnbuckles allowed the lower leg attachments and the ankle to move independently and freely in both the sagittal and transverse planes. As ankle movement in the coronal plane was minimal, the shank's attachment was not expected to cause any testing issues.
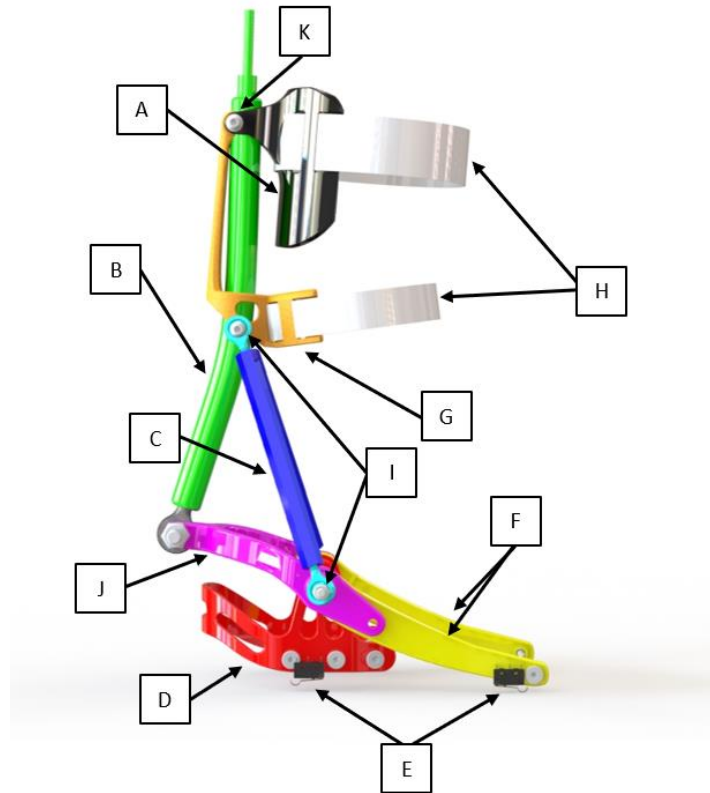
Figure 41 Labeled Diagram of AAFO Prototype.
A - Upper Shank Brace (Black), B - Pneumatic Artificial Muscle (Green), C - Adjustable Turnbuckles (Blue), D - Rear Shoe Attachment (Red), E - Tactile Switches (Black/Silver), F - Front Shoe Attachment (Yellow), G - Lower Shank Brace (Orange), H - Shank Attachment Straps (White), I - Heim Joints (Cyan), J - Leverage Arm (Pink), K - Shank Brace Pivot Pin (Grey).

The actuators used in the prototype measured 0.22 m in length when unpressurized, and when pressurized to the maximum of 483 kPa, they decreased in length to 0.17 m. The mechanism in Figure 41 weighed 0.907 kg. Figure 42 shows a comparison of the actuated and non-actuated states of the AAFO. Figure 2-A shows that the pneumatic actuator is longer and thinner in the non-actuated state than the actuated state Figure 42. It is because the soft actuator operates by expanding radially and contracting when supplied with compressed air. This forceful longitudinal contraction of the actuator is translated into a moment about the ankle through the lower actuator attachment point.

Figure 42 Comparison of Actuated and Non-actuated Prototype States.
A – Non-actuated State of the AAFO, B – Actuated State of the AAFO.

A picture of the soft-actuated AAFO prototype can be seen in Figure 43 in the configuration used for testing.



Figure 43 Picture of PAM AAFO Prototype.

5.2.2. Control

There exist various techniques to control ankle-based orthosis. (Boehler, Hollander, Sugar, & Shin, 2008) developed a stiffness-based control strategy that divided the stance phase into five zones. (Huo, Arnez-Paniagua, Ding, Amirat, & Mohammed, 2019) used an adaptive sliding mode control strategy to identify the gait phase. Precise control of the AAFO prototype was accomplished through input signals from the tactile switches fixed to the AAFO. These switches touched the ground while walking and standing and hence were actuated. While walking, the user's foot would repetitively press the tactile switches. An example of the signal sent by one AAFO during one complete gait cycle is given in Figure 44.
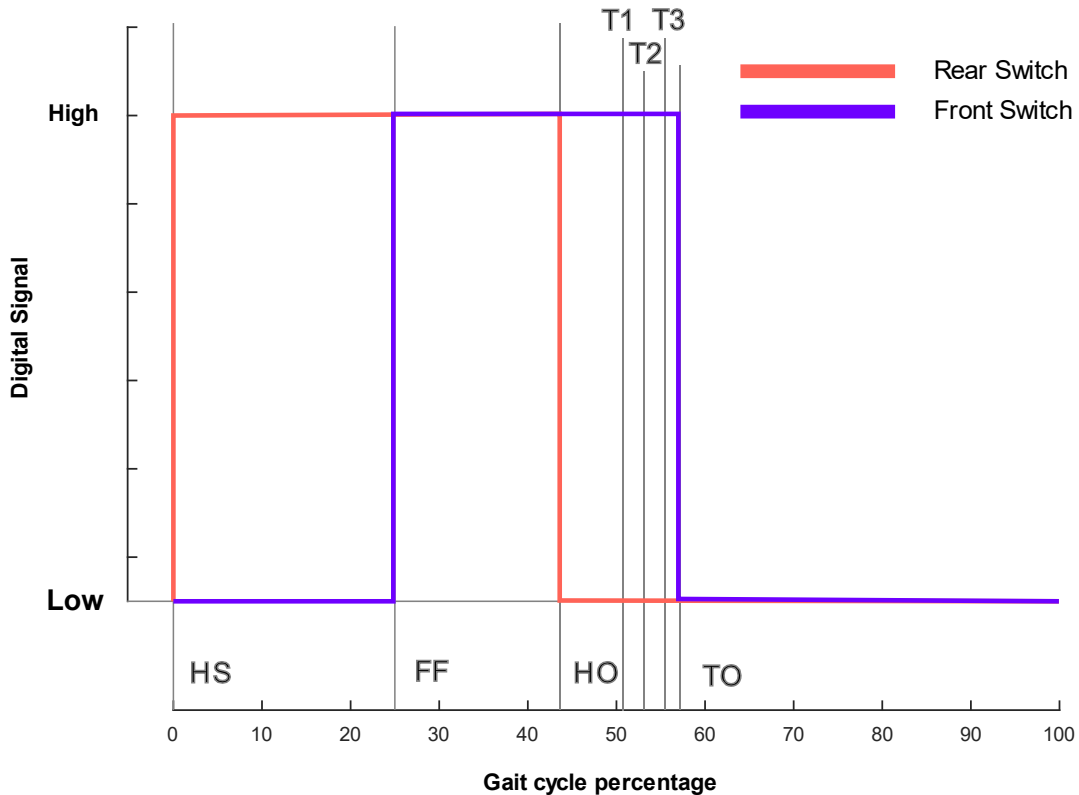


Figure 44 Exoskeleton Input Switch Signals During Walking.
T1, T2, and T3 Are the Times of the Actuation of the Mckibben Actuator. At the bottom of the Data Are Indicators of Different Sections of the Gait Cycle, Which Are Determined. "HS" Indicates the "Heel Strike" of the User, "FF" Indicates "Flat Foot," "HO" Indicates "Heel Off," and "TO" Indicates "Toe Off."

The microcontroller monitored this digital signal, with high and low values representing the depressed or non-depressed states of the AAFO switches. The front switch signal can be seen in red, and the rear switch signal in blue. From left-to-right, the plot starts with Heel Strike (HS), where the rear switch signal climbs from low to high. This indicates that the heel has contacted the ground, and the rear switch is being depressed. From there, the front switch goes from low to high as well, indicating the location of Flat Foot (FF). Here, The AAFO is now planted level on the ground with both front and rear switches depressed. Next is Heel Off (HO), indicated by the rear signal switching from high to low with the front switch still depressed. It is between HO and TO that the actuation would take place.

Actuation time of the AAFO was an essential factor in reaching maximum Anterior-Posterior GRF. Three timing delay values were used with hopes to achieve near-optimal actuation for walking assistance. When the signal reached T1, T2, or T3, depending on the timing value being use, the pneumatic solenoids would open, allowing a regulated flow of compressed air into either the right or left McKibben actuator. The relays used were two Pololu VNH5019 Motor Driver Carriers. Their role was to raise the 5V output signal of the Arduino to an 18.5V signal capable of powering the Numatics 236127B 24V 6Watt Solenoid valves, as well as to provide power for the microcontroller. Compressed air was supplied via an off-body industrial air compressor with an adjustable pressure regulator. All components shown in the block diagram of Figure 45, other than the compressed air supply and pressure regulator, were fixed to the subject during the testing. The microcontroller, motor driver carriers, and air solenoids were affixed to the subject via a waist belt. This was done to minimize weight located far from the center of the body. The entire setup worn by the user weighed 4.76 kg.

5.3. Experimentation

Six volunteer healthy male subjects participated in the experiments. The experiment and the protocol were as per Arizona State University's Institutional Review Board (STUDY 00009416).

The subjects were made accustomed to walking with the AAFO on a treadmill before the experiments.
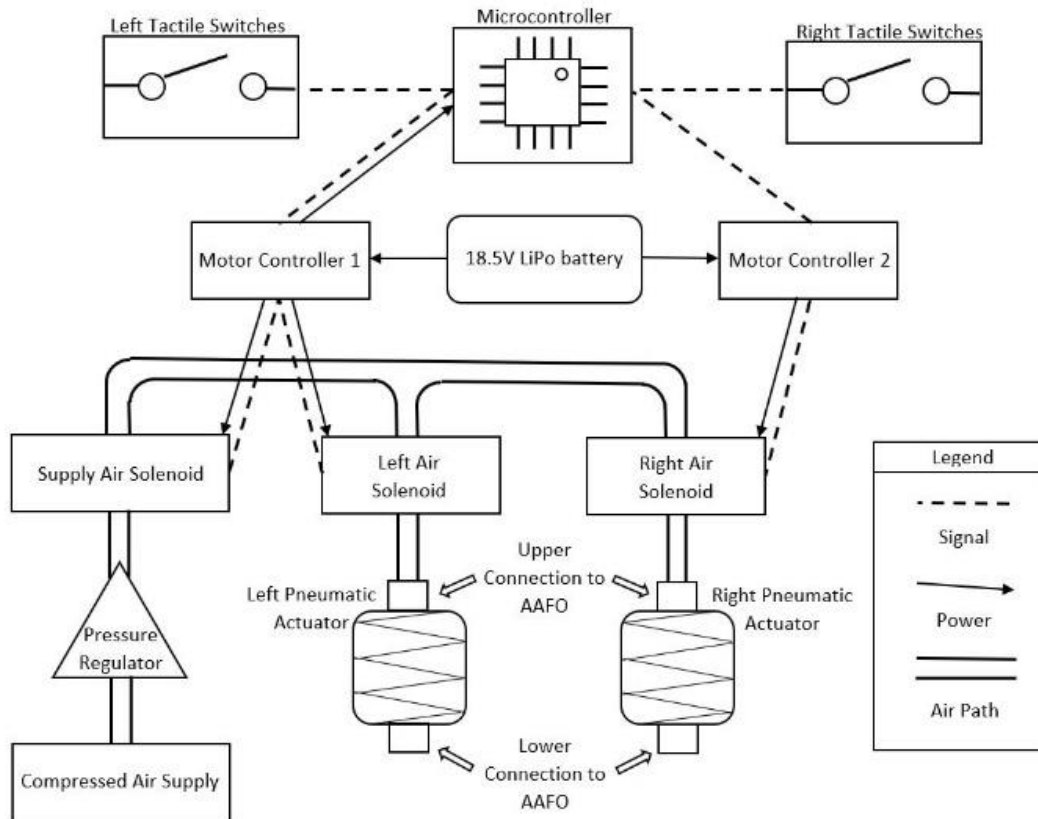


Figure 45 Block Diagram of the AAFO Prototype.
The Diagram Illustrates the Device's Significant Components and How They Are Interconnected In Power, Signal, and Airflow Paths.

The subjects were asked to walk on a Bertec Instrumented Treadmill. Ground Reaction Force (GRF) in the Z direction (positive in the vertically upward direction) and the Y direction (positive in the direction of walking) were collected. A Vicon motion capture system was used to collect kinematic and kinetic data. The subjects were equipped with retro-reflective markers based on the Newington-Helen Hayes model. The subject's muscle activity was measured using the Delsys Trigno Electromyography (EMG) sensors. The ankle angle, moment, power, muscle activity for the Gastrocnemius, the Soleus, and the Tibialis Anterior muscle groups of the leg were

61

measured. The position of the EMG sensor was determined as per the guidelines provided by the manufacturer.

5.4. Protocol

The experiment was conducted in two phases. The first phase consisted of baseline data collection and general body measurements—the mean ± standard deviation of some physical parameters for all the subjects have been listed in Table 2. The EMG data were collected during Maximum Voluntary Contractions (MVC). The subjects were asked to perform calf raises using only their left leg five times, and then they were asked to lift their toes while being loaded five times. This routine provided MVC data for the Gastrocnemius and Soleus muscle and the Tibialis Anterior muscle, respectively. The subjects were asked to walk on the treadmill while wearing the AAFO. The treadmill's speed was set to 0.5 m.s-1 and gradually increased until the subjects felt they were walking at their average pace. The treadmill was then set to 1.4 m.s-1, and the speed was gradually decreased until the subjects felt they were walking normally. The subject's normal walking speed with the device was then calculated by taking the average of the two noted speeds. The subject walked at their normal speed, and their heel-off to toe-off time was measured using the microcontroller on the AAFO and denoted the "control time."

Table 2 Mean ± Std. of the Subject's Physical Parameters

| Physical Parameters | Mean | Standard Deviation |
|---|---|---|
| Age (years) | 31.5 | 7.65 |
| Weight (kg) | 83.32 | 9.70 |
| Height (m) | 1.74 | 0.04 |
| Average Walking Speed (m.s-1) | 0.93 | 0.09 |
| Control time (ms) | 195 | 76.10 |

Phase two consisted of tests with various pressure and timing combinations. The pressure values were consistent for all subjects (207, 345, and 483 kPa), while the timing values were

different (50%, 70%, and 90% of the control time). Eleven tests combined three different pressure values, three different timing values for each pressure, no pressure, and normal walking. The list of tests and their tags are as given in Table 3. The test order was randomized for each subject. The subjects walked for two minutes on the treadmill for each test and a minute between tests at their respective average walking speeds.

Table 3 Test Tags and Descriptions

| Tag | Description |
| --- | --- |
| "Norm" | Normal walking without the suit. |
| "NoP" | Test with the subject wearing the AAFO while the AAFO was switched off/ not pressurized. |
| "P1T1" | Test with the pressure value of 207 kPa and timing value 50% of the control time. |
| "P1T2" | Test with the pressure value of 207 kPa and timing value 70% of the control time. |
| "P1T3" | Test with the pressure value of 207 kPa and timing value 90% of the control time. |
| "P2T1" | Test with the pressure value of 345 kPa and timing value 50% of the control time. |
| "P2T2" | Test with the pressure value of 345 kPa and timing value 70% of the control time. |
| "P2T3" | Test with the pressure value of 345 kPa and timing value 90% of the control time. |
| "P3T1" | Test with the pressure value of 483 kPa and timing value 50% of the control time. |
| "P3T2" | Test with the pressure value of 483 kPa and timing value 70% of the control time. |
| "P3T3" | Test with the pressure value of 483 kPa and timing value 90% of the control time. |

5.5. Post-Processing

The ankle biomechanical data were processed in Vicon's Nexus 2.0 software (Vicon Nexus 2.0, Computer Software, 2020). The EMG and GRF raw data were processed in MATLAB 2018A. A zero-phase digital Butterworth filter was used to eliminate noise (low pass second-order filter with a cut-off frequency of 5Hz). The GRF data was normalized to the subject's weight (bodyweight for normal walking and weight with the AAFO for the other tests) in Newton. The ankle moment and power were also normalized to the subject's weight in kg. The MVC data was used in the

normalization of the EMG data. The maximum absolute value of the EMG data from the MVC test was calculated. The filtered EMG data was then divided by the maximum MVC value to obtain the normalized muscle activity.

The left foot's heel and toe marker trajectories were used to obtain the heel strike, heel off, and toe-off instances. Heel strike was defined as the instance the trajectory of the heel marker in the Z direction reached its minimum value during a gait cycle. Toe-off was defined as the point where the toe marker's trajectory in the Z direction reached its minimum value during a gait cycle. The heel-off instance was determined by noting that the heel marker's z trajectory went above a certain threshold from the ground co-ordinate.

The ankle biomechanical data, GRF data, and EMG data were divided into gait cycles (heel strike to heel-strike). The data from 30 seconds to 110 seconds was considered for all the analyses. All the data were averaged over multiple gait cycles for each subject and condition. The average data were then compared and analyzed.

5.6. Statistical Analyses

The Statistical analyses were performed in R studio (R Core Team, 2019) using the package "nlme" (Pinheiro, et al., 2019) and a significance value $p < 0.05$. A Generalized Linear Mixed Model (GLMM) was used with the collected data as the dependent variable (more details in the result section) and the test conditions as the fixed effects. The subjects were random factors. A Tukey posthoc test was performed using the package "contrast" (O'Callaghan, et al., n.d.).

5.7. Results

5.7.1 Data Selection

As the goal of the AAFO was to increase horizontal push-off, the peak GRF Y values were compared for each pressure value and timing. Figure 46 shows the comparison along with the results of the statistical analyses ($F_{10,1431} = 19.3671$; $P < 0.001$). In the case of pressure value 1 (P1), the timing value T3 showed the highest peak GRF Y value (p-value < 0.01). The timing value T1 showed the highest peak GRF Y value for pressures P2 and P3. The data for P2T1 and P2T2

were not significantly different ($p < 0.2$). The same was the case with P3T1 and P3T2 ($p < 0.1$). However, in both cases, the peak values of GRF Y were higher for timing T1. Hence, normal walking (Norm), no pressure (NoP), P1T3, P2T1, and P3T1 conditions.
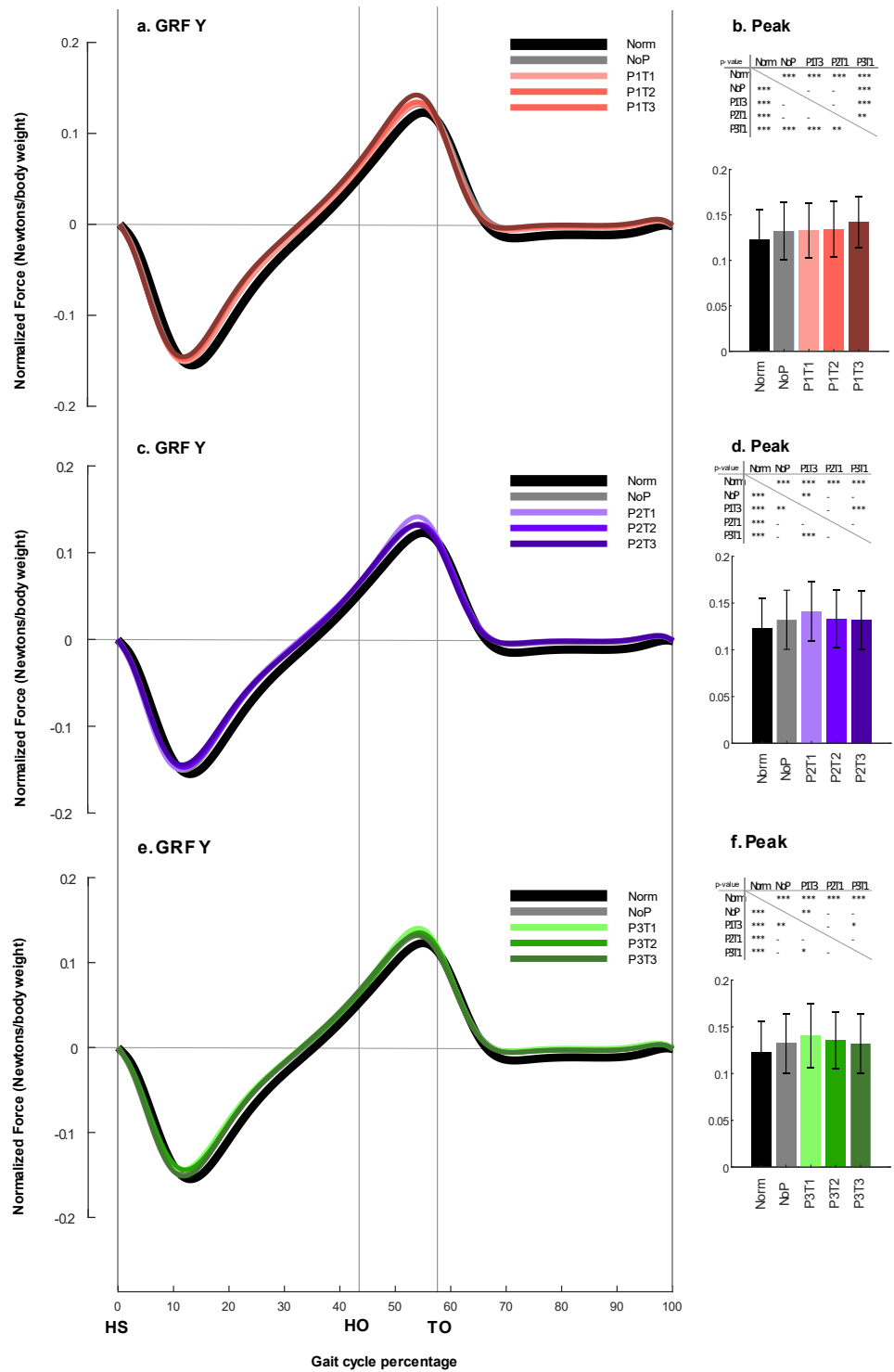
Figure 46 Ground Reaction Force Y-Direction Pressure Comparison.

a. Ground Reaction Force in the Y direction for Pressure condition 1, b. Peak GRF Y values with statistical p-value, c. Ground Reaction Force in the Y direction for Pressure condition 2, d. Peak GRF Y values with statistical p-value, e. Ground Reaction Force in the Y direction for Pressure condition 3, f. Peak GRF Y values with statistical p-value; All the bar graphs show mean ± standard deviation data; ***: $p < 0.001$, **: $p < 0.01$, *: $p <= 0.05$, -: $p > 0.05$ ;HS: Heel Strike, HO: Heel off, TO: Toe off.

### 5.7.2. Data Comparison

The data were compared at two distinct points: average over a shaded area of interest and the peak value. Statistical analyses were run for these points and were included in the manuscript. Ground Reaction Force in the Y and Z direction was compared in Figure 47. The average GRF Y value ($F_{10,1431} = 4.0383$; $P < 0.001$) for normal walking was significantly different than the other conditions ($p < 0.001$). The peak GRF Y value ($F_{10,1431} = 19.3671$; $P < 0.001$) showed a significant difference between the normal walking and no pressure conditions when compared to the pressurized conditions ($p < 0.01$).

**a. GRF Y**

**b. Average GRF Y**

| p-value | Norm | NoP | P1T3 | P2T1 | P3T1 |
|---|---|---|---|---|---|
| Norm | | *** | *** | *** | *** |
| NoP | *** | | *** | - | - |
| P1T3 | *** | *** | | - | - |
| P2T1 | *** | - | - | | |
| P3T1 | *** | - | - | | |

**c. Peak GRF Y**

| p-value | Norm | NoP | P1T3 | P2T1 | P3T1 |
|---|---|---|---|---|---|
| Norm | | *** | *** | *** | *** |
| NoP | *** | | *** | ** | ** |
| P1T3 | *** | *** | | - | - |
| P2T1 | *** | ** | - | | |
| P3T1 | *** | ** | - | | |

**d. GRF Z**

**e. Average GRF Z**

| p-value | Norm | NoP | P1T3 | P2T1 | P3T1 |
|---|---|---|---|---|---|
| Norm | | - | *** | *** | *** |
| NoP | - | | *** | * | *** |
| P1T3 | *** | *** | | ** | - |
| P2T1 | *** | * | ** | | |
| P3T1 | *** | *** | - | | |

**f. Peak GRF Z**

| p-value | Norm | NoP | P1T3 | P2T1 | P3T1 |
|---|---|---|---|---|---|
| Norm | | ** | ** | - | * |
| NoP | ** | | *** | ** | *** |
| P1T3 | ** | *** | | *** | - |
| P2T1 | - | ** | *** | | ** |
| P3T1 | * | *** | - | ** | |

Legend: Norm, NoP, P1T3, P2T1, P3T1

HS     HO     TO

Gait cycle percentage
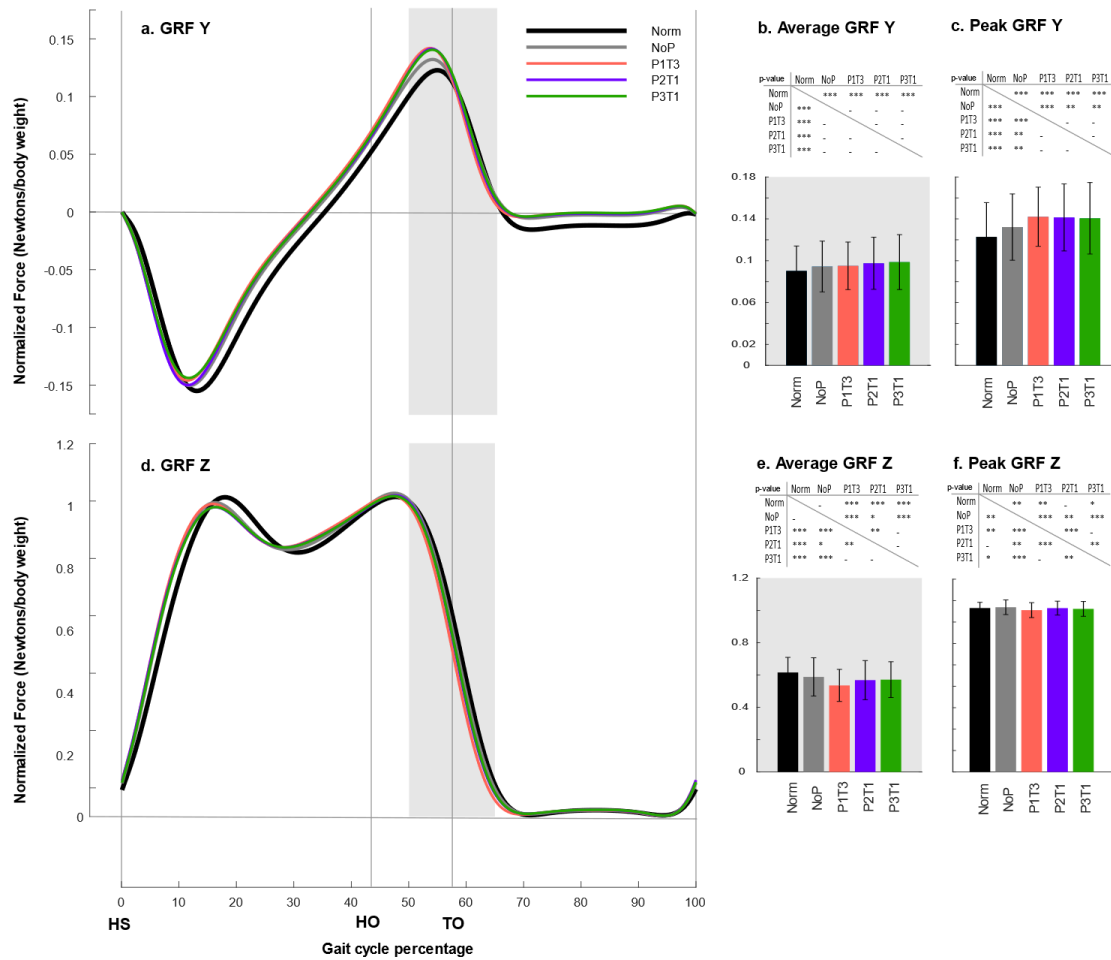
Figure 47 Ground Reaction Force Y and Z-Direction Comparison.
a. Ground Reaction Force in the Y direction, b. Average GRF Y over the shaded area with statistical p-value, c. Peak GRF Y with statistical p-value, d. Ground Reaction Force in the Z direction, e. Average GRF Z over the shaded area with statistical p-value, f. Peak GRF Z with statistical p-value; All the bar graphs show mean ± standard deviation data; ***: $p < 0.001$, **: $p < 0.01$, *: $p <= 0.05$, -: $p > 0.05$ ;HS: Heel Strike, HO: Heel off, TO: Toe off.

The P1T3 condition showed the most improvement of 15.64% in peak GRF Y compared to normal walking and an increase of 7.49% compared to the no pressure condition. The average GRF Z value ($F_{10,1431} = 7.7703$; $P < 0.001$) showed considerable decrease in P1T3 condition as compared to normal walking (13% decrease) and no pressure condition (8.9% decrease). The peak GRF Z values ($F_{10,1431} = 6.9900$; $P < 0.001$) did not show much change. Figure 48 shows a comparison between the Gastrocnemius and Soleus muscle's activities and the Tibialis Anterior

muscle activity. Average Soleus activity in the shaded area ($F_{10,1431}$ = 10.0869; $P$ < 0.001) showed a decrease of 17.8% between no pressure condition and P1T3 condition. Peak Soleus activity ($F_{10,1431}$ = 12.0034; $P$ < 0.001) showed a decrease of 14.3% between no pressure condition and P1T3 condition. Average Gastrocnemius activity in the shaded area ($F_{10,1431}$ = 11.4405; $P$ < 0.001) and peak Gastrocnemius activity ($F_{10,1431}$ = 12.4990; $P$ < 0.001) showed an increase across all conditions but the increase was not significant. Average Tibialis Anterior activity ($F_{10,1431}$ = 9.2159; $P$ < 0.001) was similar over all the conditions. Peak Tibialis Anterior ($F_{10,1431}$ = 8.1477; $P$ < 0.001) showed an increase of 6.3% between P2T1 and no pressure conditions.

**a. Soleus**

Norm
NoP
P1T3
P2T1
P3T1

Normalized Muscle Activity

**b. Average**

| p-value | Norm | NoP | P1T3 | P2T1 | P3T1 |
|---|---|---|---|---|---|
| Norm | | *** | *** | *** | *** |
| NoP | *** | | - | - | *** |
| P1T3 | *** | - | | - | * |
| P2T1 | *** | - | - | | ** |
| P3T1 | ** | *** | * | ** | |

**c. Peak**

| p-value | Norm | NoP | P1T3 | P2T1 | P3T1 |
|---|---|---|---|---|---|
| Norm | | *** | *** | *** | ** |
| NoP | *** | | * | - | *** |
| P1T3 | *** | * | | * | - |
| P2T1 | *** | - | * | | *** |
| P3T1 | ** | *** | - | *** | |

**d. Gastrocnemius**

Normalized Muscle Activity

**e. Average**

| p-value | Norm | NoP | P1T3 | P2T1 | P3T1 |
|---|---|---|---|---|---|
| Norm | | *** | *** | *** | *** |
| NoP | *** | | *** | *** | *** |
| P1T3 | *** | *** | | - | - |
| P2T1 | *** | *** | - | | - |
| P3T1 | *** | *** | - | - | |

**f. Peak**

| p-value | Norm | NoP | P1T3 | P2T1 | P3T1 |
|---|---|---|---|---|---|
| Norm | | *** | *** | *** | *** |
| NoP | *** | | ** | ** | ** |
| P1T3 | *** | ** | | - | - |
| P2T1 | *** | ** | - | | - |
| P3T1 | *** | ** | - | - | |

**g. Tibialis Anterior**

Normalized Muscle Activity

**h. Average**

| p-value | Norm | NoP | P1T3 | P2T1 | P3T1 |
|---|---|---|---|---|---|
| Norm | | * | - | *** | - |
| NoP | * | | * | *** | - |
| P1T3 | - | * | | *** | - |
| P2T1 | *** | *** | *** | | *** |
| P3T1 | - | - | - | *** | |

**i. Peak**

| p-value | Norm | NoP | P1T3 | P2T1 | P3T1 |
|---|---|---|---|---|---|
| Norm | | * | - | *** | - |
| NoP | * | | - | *** | - |
| P1T3 | - | - | | *** | - |
| P2T1 | *** | *** | *** | | *** |
| P3T1 | - | - | - | *** | |

HS          HO    TO
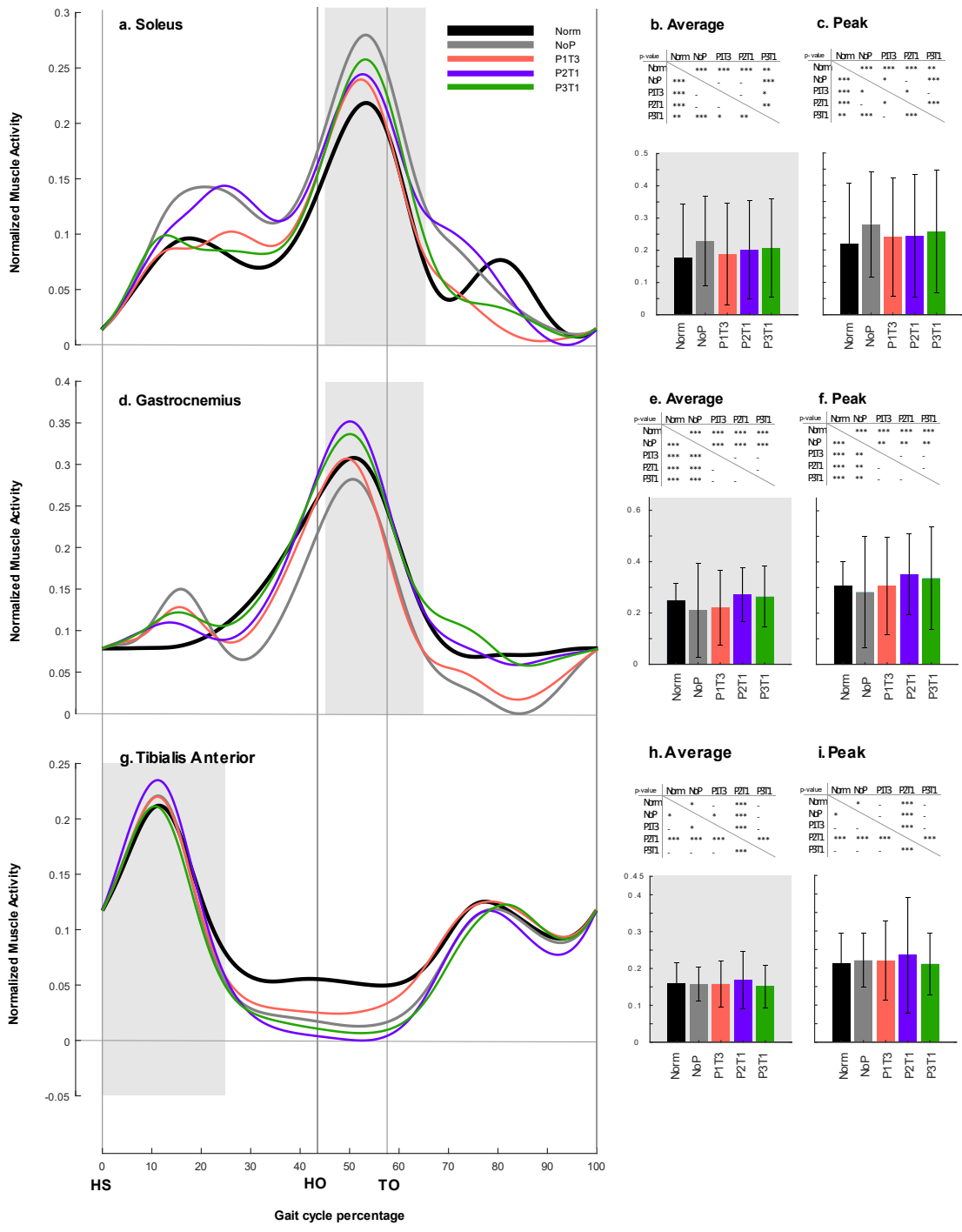
**Gait cycle percentage**

Figure 48 Soleus, Gastrocnemius and Tibialis Anterior EMG Comparison.
a. Soleus muscle activity, b. Average Soleus activity over the shaded area with statistical p-value,
c. Peak Soleus activity with statistical p-value, d. Gastrocnemius muscle activity, e. Average
Gastrocnemius activity over the shaded area with statistical p-value, f. Peak Gastrocnemius

activity with statistical p-value, g. Tibialis Anterior muscle activity, h. Average Tibialis Anterior activity over the shaded area with statistical p-value, i. Peak Tibialis Anterior activity with statistical p-value; All the bar graphs show mean ± standard deviation data; ***: $p < 0.001$, **: $p < 0.01$, *: $p <= 0.05$, -: $p > 0.05$ ;HS: Heel Strike, HO: Heel off, TO: Toe off.

The ankle biomechanical data is shown in Figure 48. Average ankle angle ($F_{10,1431} = 30.3441$; $P < 0.001$) showed a decrease around push-off (the shaded area) when compared to normal walking. The biggest significant decrease ($p < 0.05$) was seen in P3T1 (74%). The peak plantarflexion (negative ankle angle) ($F_{10,1431} = 22.0322$; $P < 0.001$) showed a significant increase of 26.64% for P3T1. Average ankle moment ($F_{10,1431} = 3.1232$; $P < 0.001$) showed a decrease of 10.3% between P1T3 and normal walking conditions ($p < 0.001$). Peak ankle moment ($F_{10,1431} = 5.1538$; $P < 0.001$) showed an increase of about 6.6% when compared to normal walking and the other conditions. Average ankle power ($F_{10,1431} = 2.6042$; $P = 0.0039$) showed an increase on about 16.6% between normal walking and P2T1 ($p < 0.001$). Peak ankle power ($F_{10,1431} = 5.9407$; $P < 0.001$) showed an increase of 14.3% between no pressure and P3T1 conditions.

5.8. Discussion

As seen in Figure 48 and Figure 49, the peak GRF data showed significant improvement for the pressurized conditions, which indicated that the push-off duration was quick in those cases. The AAFO changed the GRF Y and Z resultant direction, as seen in the butterfly curve shown in Figure 49. Gastrocnemius and Soleus muscle groups cause plantar flexion in the ankle and are also responsible for the push-off force. The activity in the Gastrocnemius muscle increased slightly. The Soleus muscle activity decreased compared to the no-pressure condition, similar to Collins et al.'s article, where they presented a passive mechanism to reduce the metabolic cost (Collins, Wiggin, & Sawicki, 2015). (Moltedo, et al., 2020) observed similar trends in their article. Their mechanism yielded a 7.2% improvement in metabolic cost and a decrease in overall Soleus activity. The mechanism was lightweight due to its passive nature. The added weight of the AAFO induced additional activity in the Soleus muscle, which was reduced considerably by the pressurized actuator.
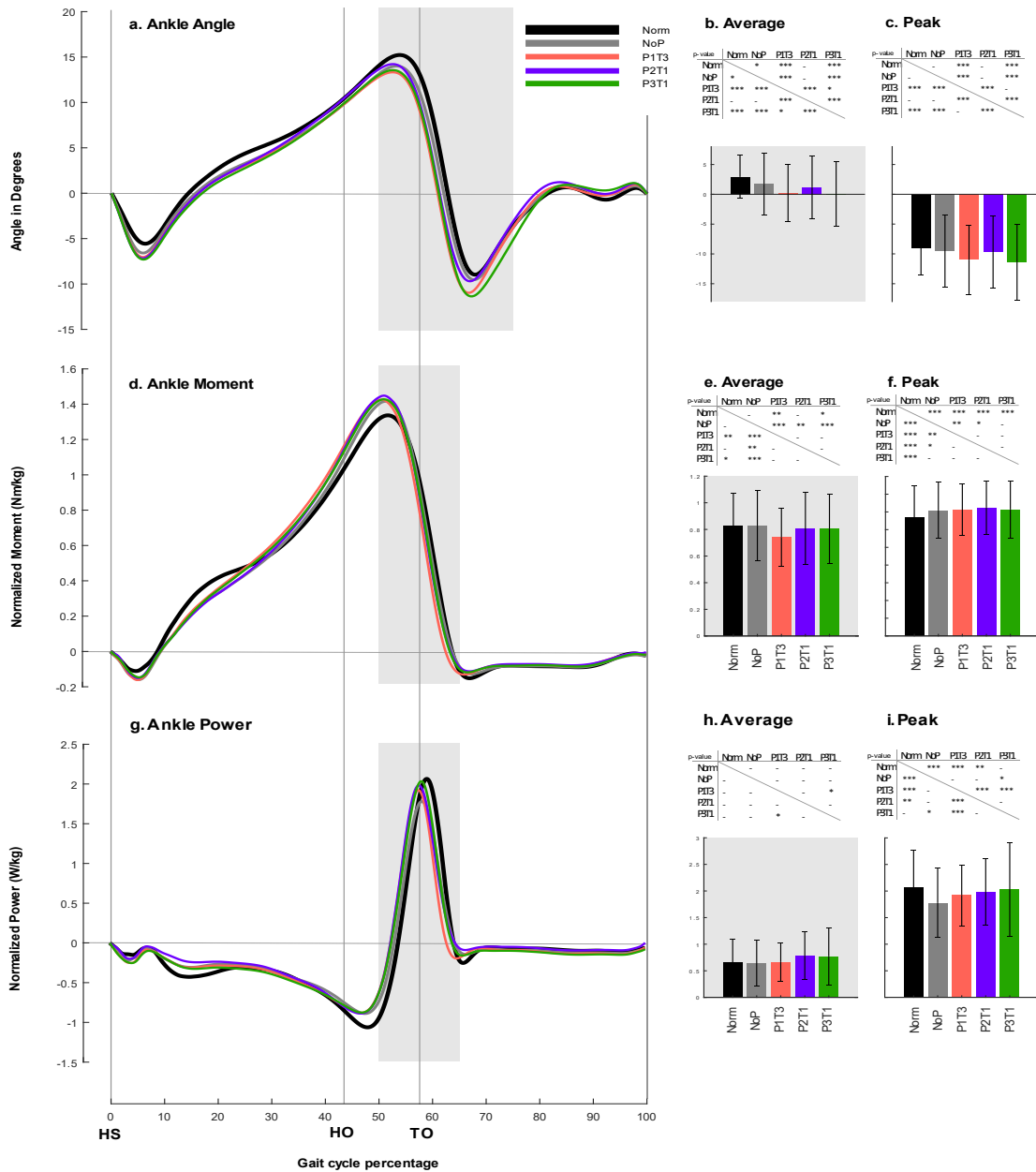
71

Figure 49 Ankle Angle, Ankle Moment and Ankle Power Comparison.
a. Ankle angle, b. Average Ankle angle over the shaded area with statistical p-value, c. Peak plantarflexion Ankle angle with statistical p-value, d. Ankle moment, e. Average Ankle moment over the shaded area with statistical p-value, f. Peak Ankle moment with statistical p-value, g. Ankle power, h. Average Ankle power over the shaded area with statistical p-value, i. Peak Ankle power with statistical p-value; All the bar graphs show mean ± standard deviation data; ***: p < 0.001, **: p < 0.01, *: p <= 0.05, -: p > 0.05 ;HS: Heel Strike, HO: Heel Off, TO: Toe Off.

The pressurized conditions showed better plantarflexion than normal walking, similar to the results in Gordon et al.'s article (Gordon, Sawicki, & Ferris, 2006). They used a higher pressure to actuate their exo-skeleton (620 kPa). Also, they did not explore the effect actuation time has on the exoskeleton. Gordon et al.'s actuators were pressurized for longer than the AAFO.

Peak ankle moment was higher for the pressurized conditions as the moment was calculated using the GRF and ankle angle data. The exciting part observed was the decrease in the average moment for the P1T3 condition. It could be attributed to the change in plantarflexion rate and observed in the GRF Y and Z data between 60% -65% gait cycle. A higher plantarflexion rate meant a rapidly decreasing moment arm as described in (Gordon, Sawicki, & Ferris, 2006). The peak ankle power decreased for the pressurized cases, but the average ankle power increased. The AAFO provided a consistent work input into the ankle joint during push-off. It decreased the amount of work done by the muscles, as observed in earlier research (Gordon, Sawicki, & Ferris, 2006).

Since the AAFO increased push-off, it can be used for fall prevention. As soon as a fall is detected, the actuator can actuate, pushing the foot forward to stop the fall. As mentioned in (Eng, Winter, & Patla, 1994), when a person trips, one strategy of fall prevention is to lower the center of mass and take a step over the obstacle. The AAFO can help in such a situation by increasing the push-off force and preventing the worker from potential injury. This AAFO could be used for strength training to increase push-off and reduce the risk of falls (Pijnappels, Bobbert, & van Dieën, 2005). Hence, the AAFO is a viable mechanism for fall prevention.

5.9. Conclusion

The article resented an AAFO design that used PAM to actuate an ankle exoskeleton at different times during push-off. It was observed that the optimum time to apply the force varied with the amount of pressure in the soft actuator. It was also noted that the lowest pressure applied at the earliest time yielded the highest amount of increase in the GRF Y push-off. The AAFO also reduced the amount of muscle activity in the Soleus. Hence, reducing the amount of effort made by the user for walking. Currently, the AAFO design is optimized for weight, power, and size. The

AAFO can potentially be used in fall prevention. A complete experiment to further explore the AAFO's application in fall prevention will be a part of future work.

Notation

GRF = Ground Reaction Force;

AAFO = Active Ankle-Foot Orthosis;

EMG = Electromyography;

P1 = pressure of actuation equal to 207 kPa;

P2 = pressure of actuation equal to 345 kPa;

P3 = pressure of actuation equal to 483 kPa;

T1 = time of actuation equal to 50% of the control time;

T2 = time of actuation equal to 70% of the control time;

T3 = time of actuation equal to 90% of the control time;

Std = Standard Deviation.

# 6 MACHINE LEARNING INTEGRATION

## 6.1. Introduction

As stated by (Han, Wang, Tian, & Christov, 2020), "stable and efficient repetitive motion control (is) the basis and most important function in lower limb exoskeleton systems." For lifting, the type of lift used to raise an object or payload steadily and efficiently would vary depending on the object's location and its unpredictable surroundings. This chapter outlines the work done to incorporate machine learning into powered exoskeletons such that they may be able to identify and act appropriately in the variety of situations in which they are needed. Although this research relates most directly to chapter three's Active-Load Carry Pulley Suit, it may in part apply to the development of all powered exoskeletons.

Most if not all powered exoskeletons possess unique requirements in actuation timing and magnitude for real-world applications. The level of control necessary to achieve commercial use of a powered exoskeleton has required machine learning. There are many different forms of machine learning which may be applicable in achieving real-world levels of control; however, the form that has been investigated in this research was the use of a neural network. A paper by (Han, Wang, Tian, & Christov, 2020) explored using a neural network to provide a time-delay estimation for use in a lower-limb rehabilitation exoskeleton. The neural network was tested in a virtual environment and, used in combination with other control strategies, was shown to improve the accuracy of the exoskeleton's tracking behavior and its ability to handle uncertainties appropriately. A similar methodology was used in pursuit of developing a neural network algorithm suitable for use in a powered lifting exoskeleton.

An essential factor for any exoskeleton design and particularly for lifting assistance is that it must not needlessly inhibit its user's abilities. For a lifting assistance exoskeleton, it must be considered that there are instances in which foreign and unpredictable circumstances may limit the type or types of lifts available. Additionally, multiple lifting types may be available to the user, in which case the user's desired lift type must be identified if the exoskeleton is to assist. An

investigation was performed to determine if a neural network would be capable of appropriately identifying different lifting types, which may be integrated into lifting assistance exoskeletons such as the A-LCPS or other powered exoskeletons.

Human subject testing was performed in which data would be collected and used to both test and validate the accuracy of the neural networking method. Neural networks require training data for both learning and validation; therefore, lifting data would be required for the investigation.
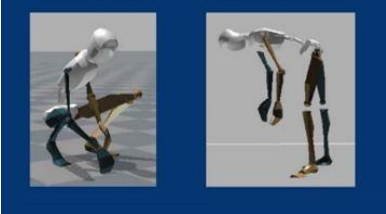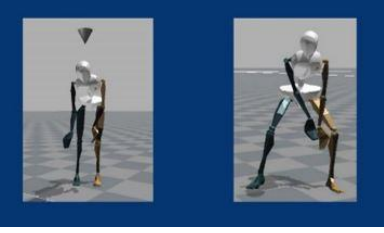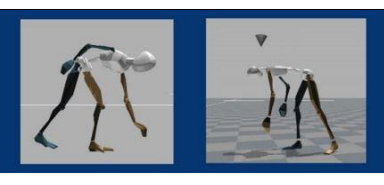
6.2. Testing

Testing was performed with six healthy subjects to acquire different types of lifting and squatting kinematic data. This data would be processed and ultimately fed into a neural network algorithm using the Neural Network Pattern Recognition tool in MATLAB's Deep Learning toolbox (MATLAB. Version 2018a, Computer Software, 2018). Kinematic data was collected via a Vicon motion capture system and was post-processed using Vicon's Nexus 2.0 software (Vicon Nexus 2.0, Computer Software, 2020). The testing procedure used included a total of 14 different lift types which were distinct in one characteristic, and all tests required subjects to lift a weight equal to 10% of their body weight. To lessen the number of tests performed, two lifting types were performed within one data capture. Approximate visual representations of the different types of lifts used in the tests can be seen in the CAD model figures on Table 4. The testing order of the seven separate captures, A through G, was randomized for each subject. For each capture, A through G, a total of ten lifts were performed, five lifts for type one and five for type two.

Following alphabetical order, test A1 asked the subject to perform a squat, with their feet shoulder-width apart, bending their knees, and keeping their chest out during the lift with the weight centered at their feet. Test A2 asked the subject to perform a stoop lift in which their knees are kept straight thru ought the lift, and the weight is centered at their feet. Test B1 asked the subject to be mindful of keeping their arms and legs symmetric thru ought the lift, with the weight being centered at their feet. Test B2 asked the subject to lift the weight being centered in front of one of the subject's legs. Test C1 asked the subject to lift the weight with two arms while keeping their legs together,

76

their feet touching, and the weight centered in front of them. Test C2 asked the subject to take a step out to either side and lift the weight from its original location from C1. Test D1 asked the subject to lift the weight centered in front of them while keeping both feet planted firmly on the ground. Test D2 asked the subject to raise one leg in bending to lift the weight which was centered in front of them. Test D2 also required subjects to lift the weight with only one arm. Test E1 asked the subject to lift the weight centered in front of them while keeping their feet parallel. Test E2 asked the subject to lift the weight centered in front of them after having taken a step back with one leg. Test F1 asked the subject to lift the weight freestyle with one hand. Test F2 asked the subject to lift the weight freestyle but using two hands. Test G1 asked the subject to lift the weight centered in front of them with both arms while keeping their feet parallel and their knees straight. Lastly, Test G2 asked the subject to lift the weight centered in front of them with one arm while keeping their feet parallel and their knees straight.

Table 4 Different Lifting Types Table Showing Each Type's Lifts and Unique Characteristics, Which Could Be Differentiated Using a Neural Network Algorithm.

| Different lifting types | |
| --- | --- |
| Test A<br><br>&bull; A1 – Squat<br><br>&bull; A2 – Stoop lift |  |
| Test B<br><br>&bull; B1 – Symmetric<br><br>&bull; B2 – Asymmetric |  |

Test C

- C1 – Legs together

- C2 – Legs apart sideways



Test D

- D1 – Both legs grounded

- D2 – One leg in air



Test E

- E1 – Legs parallel

- E2 – One leg behind



Test F

- F1 – One-handed

- F2 – Two-handed



Test G

- G1 – Lift

- G2 – Tilted lift



5 shows the mean and standard deviation of the test subjects' physical parameters. All test subjects were in good physical condition with a mean age of 29, a mean weight of 80 kilograms, and a mean height of 1.73 meters.

Table 5 Mean ± Std. of the Subject's Physical Parameters

| Physical Parameters | Mean | Standard Deviation |
|---|---|---|
| Age (years) | 29.16 | 4.35 |
| Weight (kg) | 80.85 | 17.91 |
| Height (m) | 1.73 | 0.12 |

Figure 50 shows an image of a single subject before testing. The markers used for kinematic data collection can be observed as luminous spheres located strategically around the body. The testing required using a custom marker placement configuration to ensure the cameras' view of the markers would not be blocked from the optical tracking system while squatting. Figure 51 shows a subject view with all 33 markers used during each test through Vicon's 3D Perspective view (Vicon Nexus 2.0, Computer Software, 2020).



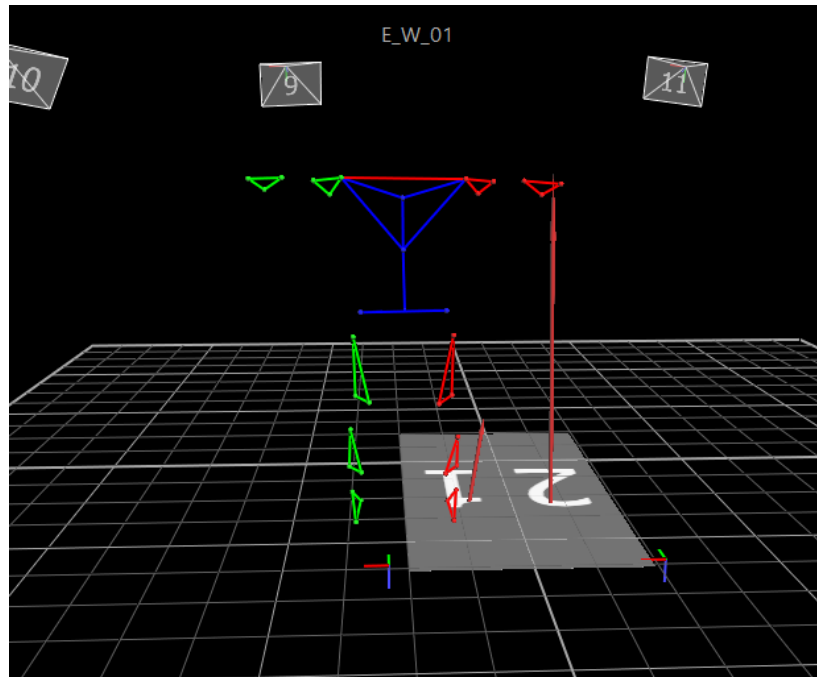Figure 50 Photo of Subject Marker Location Configuration Used in Testing.

Figure 51 3D Perspective View Showing Custom Modified 'Helen Hayes' Marker Placement
Configuration Used in Testing.
(Vicon Nexus 2.0, Computer Software, 2020).

6.3. Results

The kinematic data collected from each test was post-processed into joint-angle data for the lower-body. The plots in Figure 52 were created to illustrate the processed data collected from the testing. The plots shown are of the sagittal plane motion of the left hip, knee, and ankle of a single subject during test A1. The plot shows clear peaks for each joint angle, representing the 5 squats performed for the test, as well as the angular velocities of the joints and the phase-plane plot for each joint.
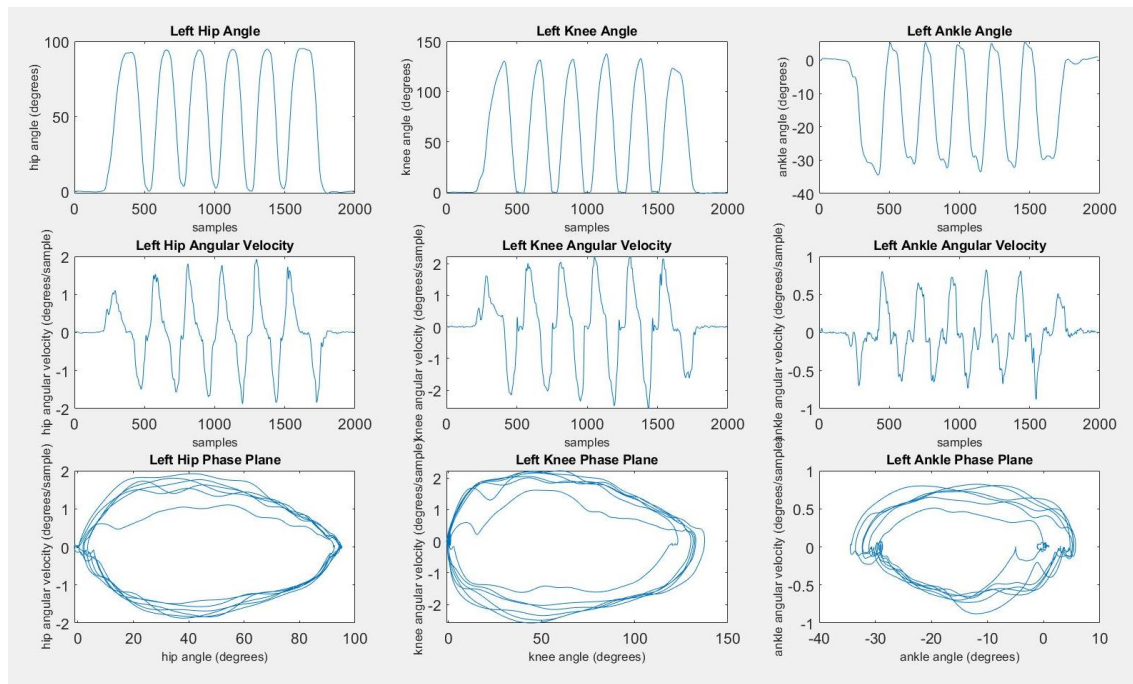
Figure 52 Hip, Knee, and Ankle Plots for Left Leg of Single A1 (Squat) Test.

The MATLAB neural network pattern recognition tool requires two matrices for implementation and training of the neural network (MATLAB. Version 2018a, Computer Software, 2018). Although both lower and upper-body kinematic data was collected, only hip, knee, and ankle data was used in creating the neural network algorithm as fewer data points would be more easily achievable from hardware and power usage standpoint. The article by (Lee, Joo, Lee, & Chee, 2020) described a classification algorithm that used different features, including maximum value and value range, for training the said algorithm. Following that approach, the max and range of the joint-angle data would be used for hips, knees, and ankles angles of each user to create the feature matrix and target matrix. For the results shown in Figure 53 and Figure 54, Different numbers of hidden layers were used to determine the best suitable neural network structure. Out of the different hidden layer quantities attempted, 50 was chosen as it achieved the highest overall accuracy value for the given data. Additional initial conditions chosen included using an 80% training ratio and a 10% ratio for both testing and validation of the algorithm. Figure 53 shows the pattern recognition neural network diagram, where the structure of the network's formation can be seen.
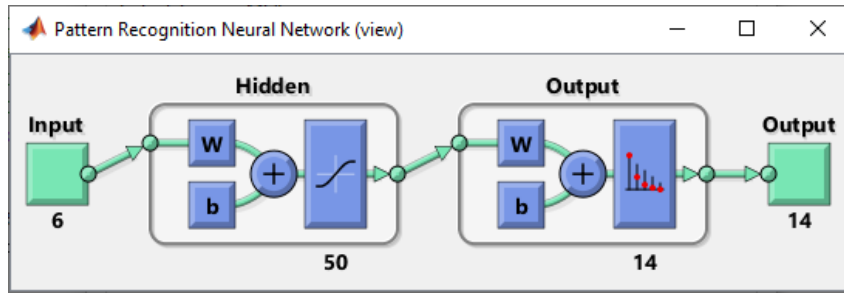
Figure 53 Pattern Recognition Neural Network Diagram.
(MATLAB. Version 2018a, Computer Software, 2018)

Figure 54 shows the confusion matrix generated using the Neural Network tool within the MATLAB Deep Learning Toolbox. The max and range values of the hip, knee, and ankle joint-angle movement were used for three out of the six subjects' data to create the confusion matrix shown in Figure 54.

Figure 54 3-Subject Confusion Matrix Plot.

6.4. Conclusion

For the analysis performed, the neural network's output showed an overall accuracy level of 84.1%. This result shows an adequate level of accuracy in identifying different features, which represented distinct lifting types. The level of differences between each lift-type varied as some lifts were much more distinct than others in terms of the max and range values being used. This can be observed in Figure 54 in that the two tested features, 9 and 13, both had an accuracy level of only 55.6%. These results correspond with tests E1 and G1, which both asked subject to perform similar, potentially identical lifts. The results highlight the need for distinct differences if a high level of accuracy is desired. Overall, the results indicate a level of accuracy in differentiating between types of lifts that could be used to provide more optimal actuation, further improving the exoskeleton's user's abilities, and empowering them to do more.

# 7 CONCLUSION

## 7.1 Summary

The first chapter of this dissertation gave a modern definition of the term "exoskeleton" and noted the earliest exoskeletons created to provide some background on their history. A literature review would follow, narrowing in on exoskeletons that addressed the same or similar goals as those discussed in this research. The second chapter focused on the development and testing of a passive squat-assistance exoskeleton named the P-LCPS. This chapter detailed the processes and refinements made to reduce unwanted friction and improve the device's performance. Metabolic data were collected on the P-LCPS and showed promising results in the form of an 11.5% reduction in metabolic costs in a non-weighted condition for squatting with the device.

Additionally, the P-LCPS created a 5.3% reduction in metabolic costs for loaded squats. Similar remarks can be made concerning the A-LCPS described in the third chapter. The chapter addressed the creation and testing of the A-LCPS, a powered exoskeleton designed for squatting assistance. The A-LCPS achieved a 16.7% reduction in the metabolic cost of squatting without additional load and a 12.5% reduction in metabolic squatting cost while lifting a 10% of body weight load. Chapters four and five addressed different versions of an AAFO exoskeleton, each with its own advantages and disadvantages.

The AAFO discussed in chapter four was tested with multiple pressure conditions, and although heavier than that of chapter five, it was shown to provide up to 116.8% increased GRF in one subject tested and did so with a straightforward algorithm for actuation. The AAFO exoskeleton discussed in chapter five used a McKibben actuator and was tested with varying pressure levels and timing delay values. The AAFO discussed in chapter five was tested to determine the best time to apply an assistive force to aid plantarflexion/ push-off. Testing results showed a decrease in the muscles' work during the powered walking tests and showed promising levels of increased push-off force, which may one day be used to prevent falls in subjects in need. Lastly, chapter six covers the testing conducted to train a neural network algorithm to identify different types of lifts by specific

characteristics or lift features. The algorithm generated yielded an 84.1% accuracy rate among the hip, knee, and angle range and max value data collected on three subjects. These results are promising and warrant further investigation into this use-case for neural networks and machine learning integration with robotic exoskeletons.

7.2 Future

Although this research has led to the progression of multiple basic design structures, each with possible clinical or commercial contributions, there is still much refinement and iteration needed to prepare any of the exoskeletons described for field implementation. At a minimum, this research may be used to further knowledge both broadly in the field of wearable technology, and more specifically, in the field of lower-body exoskeleton development. This research contains developments applicable to fellow researchers and practitioners alike, and there are specific future works relate to each exoskeleton or chapter undertaking.

The P-LCPS exoskeleton, described in chapter two, has shown promising results in terms of simplicity and effectiveness at reducing the metabolic cost of performing squats. Future studies on the P-LCPS need to collect EMG data for the legs and back of the subject while performing squatting and lifting activities to make sure that the device indeed reduces the metabolic rate for such tasks and does not translate a statistically significant workload to another muscle group. Using a tensile force transducer on the bungee should also be considered to track bungee force on future tests. Further testing is also needed to measure walking performance with an aim at metabolic savings.

Continuing with the A-LCPS discussed in chapter three, the device's weight should be reduced where possible, and protruding and snagging features should be limited. IMU drift factors would not allow for reliable long-term performance of the A-LCPS, which limited its testing ability. A sensor fusion upgrade is necessary for future walking tests to be performed, aiming at metabolic savings. Additionally, because the pulley and bungee are connected on the A-LCPS, it is capable of aiding in hip extension which may increase the capabilities and therefore, commercialization of

the A-LCPS Exoskeleton. For that reason, future work would also include investigating the A-LCPS for walking and running assistance.

Moving on to the AAFO for gait assistance, further walking tests are needed to ensure the device's actuation is suitable for walking by collecting and analyzing EMG, kinematic and Metabolic data, similar to which was done with the AAFO for fall prevention. Also, the weight of the AAFO should be reduced, along with any protruding features. Reducing weight and protruding features is an expected improvement suggestion for both gait assistance and fall-prevention AAFO devices. Future works concerning the AAFO for fall prevention include improvising an early-fall-detection method to conduct fall recovery testing. A method of advanced input pressure control should be investigated to determine the effects of incremental or multi-stage pressurization of the AAFO on EMG muscle response.

Finally, the last chapter described the research done on machine learning integration for exoskeletons, specifically in identifying different squatting and lifting characteristics. The testing and results shown were only for proof of concept, showing that the Shallow Neural Network was capable of a relatively high level of accuracy under ideal conditions. Future research requires the development of an algorithm capable of identifying different lift-types in real-time. It would also need to be integrated on an active exoskeleton, such as that of the A-LCPS, and use "Pre-determined actuation responses tailored to each lift-type. This research merely started the investigation, and future work would involve applying the algorithm generated to a lower-body exoskeleton for testing. And lastly, the use of a Shallow Neural Network as described here should be compared with other traditional and hybrid machine learning algorithms, including Deep Neural Network, Convoluted Neural Network (CNN), and Support-vector Machine (SVM). It is hoped that the research contained within this dissertation may be valuable in advancing knowledge in the appropriate fields and that the future works outlined may someday be conducted.

7.3 Potential Contribution Impact and Reach

Now that we have discussed the research performed for this dissertation, we can discuss the potential contribution, impact, and reach of this research. This research's desired contribution was the creation of effective assistive devices usable for walking, squatting, fall prevention, and rehabilitation purposes. The desired impact of this research includes improved mobility for those lacking, fall prevention for those at risk, and reduced injury, and increased productivity in careers involving manual labor. This research relates to fields including that of lower-body exoskeletons, wearable robotics, and rehabilitation. It is hoped that this research may lead to the betterment and proliferation of wearable exoskeletons, changing lives for the better.

REFERENCES

Abdoli-E, M., & Stevenson, J. M. (2007). The effect of on-body lift assistive device on the lumbar 3D dynamic moments and EMG during asymmetric freestyle lifting. *Clinical Biomechanics*, 372-380.

Abdoli-E, M., Agnew, M. J., & Stevenson, J. M. (2005). An on-body personal lift augmentation device (PLAD) reduces EMG amplitude of erector spinae during lifting tasks. *Clinical Biomechanics*, 456-465.

*AFOs* . (2014, 11 17). (Alimed) Retrieved 8 8, 2019, from https://www.alimed.com/afo-info-blog/

Asbeck, A. T., DeRossi, S. M., Holt, K. G., & Walsh, C. J. (2015). A Biologically Inspired Soft Exosuit for Walking Assistance. *The International Journal of Robotics Research (IJRR), 34*(6), 744 - 762.

Asbeck, A. T., Dyer, R. J., Larusson, A. F., & Walsh, C. J. (2013). Biologically-inspired Soft Exosuit. *IEEE International Conference on Rehabilitation Robotics.* Seattle: IEEE Xplore.

Asbeck, A. T., Schmidt, K., & Walsh, C. J. (2015). Soft exosuit for hip assistance. *Robotics and Autonomous Systems, 73*, 102 - 110.

Baltrusch, S. J., van Dieen, J. H., Bruijn, S. M., Koopman, A. S., van Bennekom, C. A., & Houdijk, H. (2019). The effect of a passive trunk exoskeleton on metabolic costs during lifting and walking. *Ergonomics*, 903-916.

Baltrusch, S. J., van Dieen, J. H., van Bennekom, C. A., & Houdijk, H. (2018). The effect of a passive trunk exoskeleton on functional performance in healthy individuals. *Applied Ergonomics*, 94-106.

Barling, J., Kevin, K. E., & Iverson, R. D. (2003). Accidental outcomes: Attitudinal consequences of workplace injuries. *Journal of Occupational Health Psychology, I*(1), 74-85.

Batchelor, F. A., Mackintosh, S. F., Said, C. M., & Hill, K. D. (2012). Falls after stroke. *International Journal of Stroke, 7*(6), 482-490.

Batchelor, F., Hill, K., Mackintosh, S., & Said, C. (2009). What Works in Falls Prevention After Stroke? A systematic Review and Meta-Analysis. *American Heart Association journals*, 1715 - 1722.

Boehler, A. W., Hollander, K. W., Sugar, T. G., & Shin, D. (2008). Design, implementation and test results of a robust control method for a powered ankle foot orthosis (AFO). *2008 IEEE International Conference on Robotics and Automation.* Pasadena.

Brockway, J. (1987). Derivation of formulas used to calculate energy - expenditure in man. . *Human Nutrition-Clinical Nutrition, 41*, 463 - 471.

Centers for Disease Control and Prevention. (n.d.). *Stroke Facts.* (U.S. Department of Health & Human Services) Retrieved 08 07, 2020, from https://www.cdc.gov/stroke/facts.htm

Chin, R., Hsiao-Wecksler, E. T., Loth, E., Kogler, G., Manwaring, S. D., Tyson, S. N., . . . Gilmer, J. N. (2009). A pneumatic power harvesting ankle-foot orthosis to prevent foot-drop. *Journal of NeuroEngineering and Rehabilitation, 6*, 19.

Cole, M. H., & Grimshaw, P. N. (2002). Low back pain and lifting: A review of epidemiology and aetiology. *Work*, 173-184.

Collins, S. H., Wiggin, M. B., & Sawicki, G. S. (2015). Reducing the energy cost of human walking using an unpowered exoskeleton. *Nature International Journal of Science, 522*, 212 - 226.

*Cosmed K5.* (2019). (Cosmed) Retrieved 2 20, 2020, from https://www.cosmed.com/en/products/cardio-pulmonary-exercise-test/k5

De La Fuente, J., Subramanian, S. C., G.Sugar, T., & Redkar, S. (2020). A robust phase oscillator design for wearable robotic systems. *Robotics and Autonomous Systems, 128.*

Deng, M.-y., Ma, Z.-y., Wang, Y.-n., Wang, H.-s., Zhao, Y.-b., Wei, Q.-x., . . . Yang, C.-j. (2019). Fall preventive gait trajectory planning of a lower limb rehabilitation exoskeleton based on capture point theory. *Frontiers of Information Technology & Electronic Engineering*, 1322-1330.

EDUEXO. (2018, January). *A Brief History of Robotic Exoskeletons*. Retrieved from EDUEXO the robotic exoskeleton kit: https://www.eduexo.com/resources/articles/exoskeleton-history/

Eng, J. J., Winter, D. A., & Patla, A. E. (1994). Strategies for recovery from a trip in early and late swing during human walking. *Experimental Brain Research*(102), 339-349.

Evans, W. (2019). *Ruthless Quotas at Amazon Are Maiming Employees*. (The Atlantic) Retrieved 02 20, 2020, from https://www.theatlantic.com/technology/archive/2019/11/amazon-warehouse-reports-show-worker-injuries/602530/

Ferris, D. P., Czerniecki, J. M., & Hannaford, B. (2005). An Ankle-Foot Orthosis Powered by Artificial Pneumatic Muscles. *Journal of Applied Biomechanics*, 189-197.

Ferris, D. P., Czerniecki, J. M., & Hannaford, B. (n.d.). An Ankle-Foot Orthosis Powered by Artificial Pneumatic Muscles.

*Gait*. (n.d.). (Physiopedia) Retrieved August 10, 2019, from https://www.physio-pedia.com/Gait

Geurts, A. C., de Haart, M., van Nes, I. J., & Duysens, J. (2005). A review of standing balance recovery from stroke. *Gait Posture, 22*(3), 267-281.

Gordon, K. E., Sawicki, G. S., & Ferris, D. (2006). Mechanical performance of artificial pneumatic muscles to power an ankle-foot orthosis. *Journal of Biomechanics*(39), 1832-1841.

Graham, R. B., Agnew, M. J., & Stevenson, J. M. (2009). Effectiveness of an on-body lifting aid at reducing low back physical demands during an automotive assembly task: assessment of EMG response and user acceptability. *Applied Ergonomics*, 936-942.

Grazi, L., Trigili, E., Proface, G., Giovacchini, F., Crea, S., & Vitiello, N. (2020). Design and Experimental Evaluation of a Semi-Passive Upper-Limb Exoskeleton for Workers With

Motorized Tuning of Assistance. *IEEE Transactions on Neural Systems and Rehabilitation Engineering, 28*(10), 2276-2285.

Groner, C. (2011, January ). *AFO users must rethink concept of 'normal' gait*. Retrieved from Lower Extremity Review: https://lermagazine.com/article/afo-users-must-rethink-concept-of-normal-gait

Ha, K. H., Varol, H. A., & Goldfarb, M. (2011, January). Volitional Control of a Prosthetic Knee using Surface Electromyography. *IEEE Transactions On Biomedical Engineering*, pp. 144-151.

Han, S., Wang, H., Tian, Y., & Christov, N. (2020). Time-delay estimation based computed torque control with robust adaptive RBF neural network compensator for a rehabilitation exoskeleton. *ISA Transactions*, 171-181.

Hansen, A., Childress, D. S., & Meier, M. R. (2002). A simple method for determination of gait events. *Journal of Biomechanics*, 135–138.

Hargrove, L. J., Li, G., Englehart, K. B., & Hudgins, B. S. (2009). Principal Components Analysis Preprocessing for Improved Classification Accuracies in Pattern-Recognition-Based Myoelectric Control. *IEEE TRANSACTIONS ON BIOMEDICAL ENGINEERING*, 1407-1414.

Holgate, R., Sugar, T., Nash, A., Kianpour, J., Johnson, C. T., & Santos, E. (2017). A Passive Ankle-Foot Prosthesis With Energy Return to Mimic Able-Bodied Gait. *ASME 2017 International Design Engineering Technical Conferences and Computers and Information in Engineering Conference.* Cleveland, Ohio, USA.

Honeycutt, C. F., Nevisipour, M., & Grabiner, M. D. (2016). Characteristics and adaptive strategies linked with falls in stroke survivors from analysis of laboratory-induced falls. *Journal of Biomechanics, 49*, 3313 - 3319.

Huo, W., Arnez-Paniagua, V., Ding, G., Amirat, Y., & Mohammed, S. (2019). Adaptive Proxy-Based Controller of an Active Ankle Foot Orthosis to Assist Lower Limb Movements of Paretic Patients. *Robotica, 37*(12), 2147-2164.

Hwang, S., Kim, J., Sohn, R., Lee, Y., & Kim, Y. (2006). Development of an Active Ankle Foot Orthosis to Prevent Foot Drop and Toe Drag in Hemiplegic Patients. *2006 International Conference on Biomedical and Pharmaceutical Engineering, ICBPE.* Singapore.

*Important Facts about Falls*. (2017, 2 10). (Centers for Disease Control and Prevention) Retrieved 8 10, 2019, from https://www.cdc.gov/homeandrecreationalsafety/falls/adultfalls.html

Ineichen, O. (2019, 8 13). Exoskeleton developers must keep improving capabilities, cost, says maxon manager.

Jamieson, D. (2015). *The Life and Death of an Amazon Warehouse Temp*. (The Huffington Post) Retrieved 01 07, 2021, from https://highline.huffingtonpost.com/articles/en/life-and-death-amazon-temp/

Jensen, L. K. (2008). Knee osteoarthritis: influence of work involving heavy lifting, kneeling, climbing stairs or ladders, or kneeling/squatting combined with heavy lifting. *Occupational & Environmental Medicine*, 72-89.

Kazerooni, H. (2005). Exoskeletons for human power augmentation. *IEEE/RSJ International Conference on Intelligent Robots and Systems.* Edmonton, Alta., Canada.

Keller, M. (2016, 8 25). *Do You Even Lift, Bro? Hardiman Was GE's Muscular Take On The Human-Machine Interface.* (GE Reports) Retrieved 8 15, 2019, from https://www.ge.com/reports/do-you-even-lift-bro-hardiman-and-the-human-machine-interface/

Lee, J., Joo, H., Lee, J., & Chee, Y. (2020). Automatic Classification of Squat Posture Using Inertial Sensors: Deep Learning Approach. *Sensors*, 361.

Li, R. Y., & Ping Lung Ng, D. (2017). Wearable Robotics, Industrial Robots and Construction Worker's Safety and Health. *Advances in Human Factors in Robots and Unmanned Systems, 595*, 31-36.

Malcolm, P., Derave, W., Galle, S., & De Clercq, D. (2013). A simple exoskeleton that assists plantarflexion can reduce the metabolic cost of human walking. *PloS One, 8*(2).

*Materials Handling: Heavy Lifting*. (n.d.). (United States Department Of Labor) Retrieved 8 8, 2019, from https://www.osha.gov/SLTC/etools/electricalcontractors/materials/heavy.html

MATLAB. Version 2018a, Computer Software. (2018). Natick, MA: The Math Works, Inc.,.

MECHATECH. (2019). *Exoskeletons History - part 1*. (Mechatech) Retrieved 10 21, 2020, from Mechatech: https://www.mechatech.co.uk/journal/exoskeletons-history-part-1

MECHATECH. (2019). *Exoskeletons History - part 4*. (Mechatech) Retrieved 01 04, 2021, from MECHATECH embrace technology: https://www.mechatech.co.uk/journal/exoskeleton-history-part-4

Miller, J. D., Najafi, B., & Armstrong, D. G. (2015). Current Standards and Advances in Diabetic Ulcer Prevention and Elderly Fall Prevention Using Wearable Technology. *Current Geriatrics Reports*, 249-256.

Moltedo, M., Baček, T., Serrien, B., Langlois, K., Vanderborght, B., Lefeber, D., & Rodriguez-Guerrero, C. (2020). Walking with a powered ankle-foot orthosis: the effects of actuation timing and stiffness level on healthy users. *Journal of NeuroEngineering and Rehabilitation, 17*(1), 1-15.

Mooney, L. M., & Herr, H. M. (2016). Biomechanical walking mechanisms underlying the metabolic reduction caused by an autonomous exoskeleton. *Journal of NeuroEngineering and Rehabilitation, 13*(4), 1 - 12.

Mooney, L. M., Rouse, E. J., & Herr, H. M. (2014). The autonomous exoskeleton reduces the metabolic cost of human walking during load carriage. *Journal of NeuroEngineering and Rehabilitation, 11*(1), 1-11.

MYERS, D. R., & MOSKOWITZ, G. D. (1981). Myoelectric Pattern Recognition for Use in the Volitional Control of Above-Knee Prostheses. *IEEE transactions on Systems, Man and Cybernetics*, 296-302.

Nevisipour, M. (2019). Evaluating the Effects of Ankle-Foot-Orthoses, Functional Electrical Stimulators, and Trip-specific Training on Fall Outcomes in Individuals with Stroke.

O'Callaghan, A., Kuhn, M., Weston, S., Wing, J., Forester, J., & Thaler, T. (n.d.). *A Collection of Contrast Methods*. Retrieved 01 07, 2021, from https://cran.r-project.org/package=contrast

Palmer, M. L. (2002). Sagittal plane characterization of normal human ankle function across a range of walking gait speeds.

Pijnappels, M., Bobbert, M. F., & van Dieën, J. H. (2005). Push-off reactions in recovery after tripping discriminate young subjects, older non-fallers and older fallers. *Gait Posture, 21*(4), 388-394.

Pinheiro, J., Bates, D., DebRoy, S., Sarkar, D., Heisterkamp, S., & Van Willigen, B. (2019). *Fit and compare Gaussian linear and nonlinear mixed-effects models.* Retrieved 01 07, 2021, from https://cran.r-project.org/package=nlme

Polinkovsky, A., Bachmann, R. J., Kern, N. I., & Quinn, R. D. (2012). An Ankle Foot Orthosis with Insertion Point Eccentricity Control. *IEEE/RSJ International Conference on Intelligent Robots and Systems.* Vilamoura, Portugal.

Pope, M. H. (1989). Risk indicators in low back pain. *Ann Med.* , 387-392.

Qi, H., Bone, G. M., & Zhang, Y. (2019). Position Control of Pneumatic Actuators Using Three-Mode Discrete-Valued Model Predictive Control. *Actuators, 8*(3), 56.

Quintero, D., Lambert, D. J., Villarreal, D. J., & Gregg, R. D. (2017). Realtime continuous gait phase and speed estimation from a single sensor. *2017 IEEE Conference on Control Technology and Applications (CCTA).* Mauna Lani.

R Core Team. (2019). *The R Project for Statistical Computing.* Retrieved 01 07, 2021, from http://www.r-project.org/

*Rehabilitation.* (2019, 7 1). (MedlinePlus) Retrieved 8 9, 2019, from https://medlineplus.gov/rehabilitation.html

Scheme, E., & Englehart, K. (2011). Electromyogram pattern recognition for control of powered upper-limb prostheses: State of the art and challenges for clinical use. *Journal of Rehabilitation Research and Development*, 643-660.

Singer, R., Maufroy, C., & Schneider, U. (2020). Automatic support control of an upper body exoskeleton — Method and validation using the Stuttgart Exo-Jacket. *Wearable Technologies, 1*(2).

Sugar, T., Fernandez, E., Kinney, D., Hollander, K. W., & Redkar, S. (2017). HeSA, hip exoskeleton for superior assistance. *Biosystems and Biorobotics, 16*, 319 - 323.

Taborri, J., Palermo, E., Rossi, S., & Cappa, P. (2016). Gait partitioning methods: A systematic review. *Sensors, 16*(1), 66.

Torxiri, S., Naf, M. B., Lazzaroni, M., Fernandez, J., Sposito, M., Poliero, T., . . . Ortiz, J. (2019). Back-support exoskeletons for occupational use: an overview of technological advances and trends. *IISE Transactions on Occupational Ergonomics and Human Factors, 7*, 237-249.

Varol, H. A., Sup, F., & Goldfarb, M. (2010). Multiclass Real-Time Intent Recognition of a Powered Lower Limb Prosthesis. *IEEE TRANSACTIONS ON BIOMEDICAL ENGINEERING*, 542-551.

Verrusio, W., Gianturco, V., Cacciafesta, M., Marigliano, V., Troisi, G., & M., R. (2017). Fall prevention in the young old using an exoskeleton human body posturizer: a randomized controlled trial. *Aging Clinical and Experimental Research*, 207-214.

Vicon Nexus 2.0, Computer Software. (2020). Hauppague, NY: Vicon Industries, Inc.,.

Vidya K. Nandikolla, R. B. (2017). Experimental Gait Analysis to Study Stress Distribution of the Human Foot. *Journal of medical engineering, 2017*, 1-13.

Waddell, G., & Burton, A. K. (2001). Occupational health guidelines for the management of low back pain at work: evidence review. *Occupational Medicine, 51*(2), 124-135.

Wang, S., Jiaxing, S., & Shuwen, L. (2021). Fall prevention system based on airbag protection and mechanical exoskeleton support. *MATEC Web of Conferences.*

Watanabe, T., Saito, H., Koike, E., & Nitta, K. (2011). A preliminary test of measurement of joint angles and stride length with wireless inertial sensors for wearable gait evaluation system. *Comput Intell Neurosci. , 2011*, 411-422.

Weerdesteyn, V., de Niet, M., van Duijnhoven, H. J., & Geurts, A. C. (2008). Falls in individuals with stroke. *Journal of Rehabilitation and Development, 45*(8), 1195-1213.

Wehner, M., Quinlivan, B., Aubin, P. M., Martinez-Villalpando, E., Baumann, M., Stirling, L., . . . Walsh, C. (2013). A Lightweight Soft Exosuit for Gait Assistance. *IEEE International Conference of Robotics and Automation (ICRA).* Karlsruhe, Germany.

Wehner, M., Rempel, D., & Kazerooni, H. (2009). Lower Extremity Exoskeleton Reduces Back Forces in Lifting. *ASME 2009 Dynamic SYstems and Control Conference.* Hollywood: ASME.

*What is an exoskeleton?* (2019, January 27). Retrieved from Exoskeletonreport: https://exoskeletonreport.com/what-is-an-exoskeleton/

Yamamoto, S., Ebina, M., Miyazaki, S., Kawai, H., & Kubota, T. (1997). Development of a New Ankle-Foot Orthosis with Dorsiflexion Assist, Part 1: Desirable Characteristics of Ankle-Foot Orthoses for Hemiplegic Patients. *JPO Journal of Prosthetics and Orthotics, 9*(4), 174-179.

Yildirim, Y., Gunay, S., & Karadibak, D. (2014). Identifying factors associated with low back pain among employees working at a package producing industry. *Journal of Back and Musculoskeletal Rehabilitation, 27*(1), 25-32.

YOUNG, A. J., SIMON, A. M., FEY, N. P., & HARGROVE, L. J. (2014). Intent Recognition in a Powered Lower Limb Prosthesis Using Time History Information. *Annals of Biomedical Engineering*, 631-641.

Young, A. J., Simon, A., & Hargrove, L. J. (2013). An Intent Recognition Strategy for Transfemoral Amputee Ambulation Across Different Locomotion Modes. *IEEE EMBS* (pp. 1587-1590). Osaka, Japan : IEEE.

Yu, S., Huang, T.-H., Wang, D., Lynn, B., Sayd, D., Silivanov, V., . . . Yingli Tian, H. S. (2019). Design and Control of a Quasi-Direct Drive Soft Exoskeleton for Knee Injury Prevention during Squatting. *Institute of Electrical and Electronics Engineers (IEEE)*.

Zhang, F., Dou, Z., Nunnery, M., & Huang, H. (2011). Real-time Implementation of an Intent Recognition System for Artificial Legs. *IEEE EMBS* (pp. 2997-3000). Boston, Massachusetts, USA: IEEE.

Zhang, F., Liu, M., & Huang, H. (2015). Effects of Locomotion Mode Recognition Errors on Volitional Control of Powered Above-Knee Prostheses. *IEEE transactions on neural systems and rehabilitation engineering*, 64-72.

Zhang, X., Huang, H., & Yang, Q. (2012). Implementing an FPGA system for real-time intent recognition for prosthetic legs. *Design Automation Conference* (pp. 169-175). San Francisco, CA, USA: IEEE.